



OPEN Behavior-aware energy management in microgrids using quantum-classical hybrid algorithms under social and demand dynamics

Liu Minghong¹, Fu Gaoshan², Wang Pengchao¹, Yuan Xin¹, Li Qing¹, Tengfei Hou³✉ & Zhang Shuo³

The increasing intricacy of modern microgrids, driven by uncertain consumption patterns, decentralized renewables, and user behavioral dynamics, calls for innovative optimization methodologies. This study introduces a hybrid quantum-classical framework for demand-side energy management, leveraging behavioral modeling to foster resilience and flexibility. By embedding principles from Social Cognitive Theory—such as behavioral imitation, confidence in personal capability, and social reinforcement—into a multi-objective optimization scheme, the model supports distributed decision-making and promotes adaptive prosumer behavior. The proposed approach employs Quantum Annealing in combination with NSGA-III to efficiently navigate the complex solution space, accounting for real-time uncertainties and the stochastic nature of both demand and renewable supply. The framework is tested within a case study of a peer-to-peer microgrid network, showcasing its effectiveness in enhancing energy efficiency, lowering peak demand, and improving operational resilience. Performance comparisons with traditional methods, including Mixed-Integer Programming and conventional metaheuristics, underline the improved scalability and robustness of the quantum-inspired model in handling trade-offs between cost, reliability, and socially-driven demand response. The research highlights the potential of integrating quantum-inspired optimization with behavioral energy modeling to advance intelligent and socially-responsive microgrid control systems.

Keywords Quantum-inspired optimization, Social cognitive theory, Behavioral demand response, NSGA-III, Quantum annealing, Microgrid resilience enhancement, Behavioral energy management

The accelerating integration of renewable energy technologies and the pressing demand for sustainable energy solutions have positioned microgrids as a cornerstone of contemporary power infrastructure¹. Functioning as decentralized energy systems, microgrids can seamlessly operate either in isolation or alongside the central grid, delivering key benefits such as improved system resilience, enhanced energy autonomy, and flexible resource utilization². Nonetheless, the growing dependence on variable renewable sources like wind and solar poses considerable operational hurdles, primarily due to their non-dispatchable and uncertain nature^{3,4}. To maintain stable and optimal microgrid performance under these volatile conditions, there is a critical need for intelligent optimization mechanisms capable of responding in real time to changes in both generation and consumption, while simultaneously addressing technical constraints, economic efficiency, and user-driven factors⁵.

The conventional optimization of microgrid operations typically relies on classical optimization techniques such as mixed-integer programming, heuristic algorithms, and metaheuristic approaches like particle swarm optimization and genetic algorithms. While these methods have demonstrated effectiveness in certain applications, they often struggle with scalability, real-time adaptability, and multi-objective trade-offs inherent in modern energy systems^{6,7}. Additionally, they lack the ability to integrate behavioral influences and policy-driven incentives, which are increasingly recognized as crucial components in shaping energy consumption

¹State Grid Xinjiang Economic Research Institute, Ürümqi, Xinjiang, China. ²State Grid Xinjiang Electric Power Co. Ltd., Ürümqi, Xinjiang, China. ³School of Automation, Nanjing University of Science and Technology, Nanjing, China. ✉email: tengfeihou@njjust.edu.cn

patterns and optimizing demand-side management strategies. Given these limitations, there is a growing need for innovative optimization frameworks that can address the computational complexity of large-scale microgrid operations while simultaneously integrating technical, economic, and social dimensions⁸.

Although significant advances have been made in classical optimization techniques for microgrid energy management, existing methods often struggle to efficiently solve large-scale, behavior-aware, multi-objective problems due to the combinatorial complexity and high-dimensional search spaces involved. Furthermore, the dynamic and uncertain nature of user behavior under varying pricing and incentive schemes introduces additional challenges that require both exploration and exploitation capabilities in optimization. Quantum-inspired optimization methods offer promising advantages in terms of convergence speed and global search ability, but purely quantum systems are currently constrained by hardware limitations. Thus, hybrid quantum-classical frameworks present an effective compromise, leveraging quantum-inspired exploration mechanisms within classical computational infrastructures to address complex, behavior-driven control challenges in microgrid environments. Motivated by these technical gaps and practical needs, this study proposes a novel hybrid optimization approach that integrates social cognition modeling with quantum-classical search dynamics. To address these gaps, recent studies have highlighted the importance of dynamic behavior modeling⁹, real-time policy adaptation, and the application of quantum-inspired methods in energy management, which collectively support the need for a more integrated and adaptive optimization framework¹⁰. This paper introduces a novel quantum-inspired optimization (QIO) framework that integrates Social Cognitive Theory (SCT) and dynamic policy mechanisms to enhance the sustainability, resilience, and economic feasibility of microgrid operations. The proposed framework leverages QIO principles such as quantum annealing, tunneling, and entanglement to efficiently navigate complex multi-objective optimization landscapes. Unlike classical methods that often become trapped in local optima, QIO facilitates global search efficiency, enabling superior optimization of microgrid functions, including energy generation, storage management, and demand-side incentives. Beyond its technical superiority, the proposed methodology is distinguished by its integration of behavioral and policy considerations. SCT provides a theoretical foundation for modeling user behavior and participation in energy management programs. By incorporating behavioral incentives such as gamified rewards, social learning effects, and dynamic tariff structures, the optimization framework encourages energy-saving behaviors and enhances the overall engagement of microgrid users. Additionally, the framework employs adaptive subsidy mechanisms and real-time pricing strategies to align economic incentives with sustainability goals. This combination of QIO, behavioral modeling, and dynamic policy design represents a significant departure from traditional microgrid optimization approaches, positioning this study at the forefront of next-generation energy management solutions.

A key distinguishing feature of this study is its ability to address the trade-offs between economic, environmental, and social objectives in a holistic manner. Unlike traditional approaches that focus solely on cost minimization or renewable energy maximization, the proposed framework balances multiple conflicting objectives by leveraging Pareto-based optimization strategies. This ensures that microgrid operation is not only cost-effective but also aligned with long-term sustainability goals. Moreover, the quantum-inspired resilience metric embedded in the framework enhances the microgrid's ability to withstand cyber-physical disturbances, ensuring that energy supply remains stable even in the face of adversarial threats or extreme weather events. To validate the effectiveness of the proposed optimization framework, a comprehensive case study is conducted on a rural microgrid system with diverse energy resources, including solar, wind, and hybrid storage technologies. Synthesized data is used to simulate varying energy demand patterns, policy constraints, and user participation scenarios. The results demonstrate that the QIO-based approach significantly outperforms conventional methods in terms of computational efficiency, renewable energy utilization, and user engagement. Specifically, the framework achieves a more optimal balance between life-cycle costs, carbon footprint reduction, and system resilience, showcasing its potential for real-world deployment. The primary contributions of this study can be summarized as follows.

First, it introduces a novel quantum-inspired optimization framework tailored for microgrid operations, leveraging quantum annealing and tunneling mechanisms to enhance solution efficiency.

Second, it integrates Social Cognitive Theory into microgrid optimization, enabling a more accurate representation of user behavior and demand-side participation.

Third, it incorporates dynamic policy mechanisms such as real-time adaptive tariffs and behavioral incentives to align microgrid economic performance with sustainability objectives.

Finally, the study develops a quantum-informed resilience metric that ensures stable microgrid operation under uncertain and adversarial conditions. These contributions collectively position this research as a pioneering effort in the field of intelligent and sustainable energy management.

Literature review and research gaps

Microgrid optimization has traditionally employed a range of techniques, including deterministic methods (e.g., mixed-integer linear programming), stochastic optimization approaches (e.g., scenario-based and probabilistic models), robust optimization methods (e.g., worst-case formulations), and metaheuristic algorithms such as genetic algorithms and particle swarm optimization¹¹. These methods have been widely applied to optimize energy dispatch, storage utilization, and demand-side management. Deterministic approaches provide exact solutions but often fail to handle real-time uncertainties, particularly in renewable energy generation¹². Stochastic optimization improves upon this by considering probabilistic uncertainties, but it requires a high computational burden and depends on well-defined probability distributions¹³. Metaheuristic approaches offer greater flexibility and scalability, yet they lack guarantees of global optimality and often require extensive tuning of algorithm parameters. While these methods have demonstrated effectiveness in various microgrid

applications, they struggle with the combinatorial complexity and real-time adaptability required for large-scale, multi-objective optimization¹⁴.

To overcome these limitations, researchers have explored hybrid approaches that integrate machine learning with classical optimization. Reinforcement learning has been increasingly applied to demand response management, energy pricing strategies, and grid stability enhancement¹⁵. These learning-based methods offer adaptive decision-making capabilities and can efficiently capture nonlinear relationships within microgrid operations. However, they typically require extensive training data and can suffer from instability in dynamic environments¹⁶. Deep reinforcement learning, which combines deep neural networks with reinforcement learning techniques, has been proposed to improve policy generalization¹⁷. Nevertheless, these models remain computationally expensive and may not always guarantee convergence to an optimal solution. Despite these advancements, the need for optimization frameworks that efficiently handle uncertainty, high-dimensional decision spaces, and multiple conflicting objectives remains largely unmet¹⁸.

Parallel to advancements in optimization techniques, there has been growing recognition of the importance of incorporating user behavior into microgrid operation models. SCT has been widely studied in energy consumption behavior modeling, particularly in demand response programs and energy efficiency interventions^{19,20}. SCT emphasizes the role of social influence, self-efficacy, and environmental reinforcement in shaping user decisions. Empirical studies have shown that behavioral incentives such as peer comparisons, gamification, and dynamic pricing significantly impact energy consumption patterns^{21,22}. These findings underscore the need to integrate behavioral models into microgrid optimization to improve demand-side participation. However, existing research largely treats behavioral incentives as static parameters rather than dynamic components that evolve based on real-time user interactions. The challenge remains in designing an optimization framework that dynamically adapts behavioral incentives to achieve energy efficiency while maintaining economic and operational stability²³.

In addition to behavioral incentives, policy mechanisms play a crucial role in microgrid operation and expansion. Traditional policy-driven optimization frameworks incorporate static subsidy structures and tariff mechanisms to promote renewable energy adoption and demand-side management²⁴. However, these approaches often fail to account for real-time market fluctuations and evolving consumer behaviors. Dynamic pricing schemes and adaptive subsidy allocations have been proposed to address this issue, allowing electricity prices and financial incentives to respond to grid conditions in real time. Despite these efforts, a major gap in the literature remains in developing an integrated policy-technical framework that simultaneously optimizes microgrid operations while dynamically adjusting policy mechanisms. The interplay between user engagement, economic incentives, and technical constraints is highly complex and requires a multi-disciplinary approach that bridges behavioral economics, energy policy, and advanced optimization²⁵.

Recent advancements in QIO have opened new avenues for addressing the computational challenges inherent in microgrid optimization. Unlike classical approaches, which sequentially evaluate solutions, QIO leverages quantum mechanics principles such as superposition, entanglement, and tunneling to explore vast solution spaces more efficiently^{26,27}. Quantum annealing, a widely studied QIO technique, has demonstrated significant computational advantages in solving large-scale combinatorial optimization problems²⁸. By allowing solutions to probabilistically transition through energy barriers rather than over them, QIO can escape local optima and achieve superior global optimization²⁹. Several studies have explored QIO applications in energy management³⁰, including smart grid scheduling, energy trading, and load balancing. While these studies have shown promising results, most have focused solely on technical optimization without considering behavioral and policy-driven dimensions. The integration of QIO with social and economic factors remains an underexplored research direction with substantial potential for improving microgrid operations³¹.

In summary, although a wide range of optimization techniques have been applied to microgrid energy management—spanning deterministic approaches, stochastic formulations, robust methods, and metaheuristic algorithms—several critical research gaps remain. First, most existing studies do not adequately model the dynamic nature of user behavior and participation in demand-side programs. Behavioral incentives are often treated as fixed parameters rather than evolving mechanisms influenced by social context, learning, or adaptive feedback, which limits the realism and responsiveness of these models. Second, while dynamic pricing and incentive schemes are recognized as important tools, few existing frameworks incorporate them in a way that is tightly coupled with behavioral modeling and system-level optimization. Third, classical optimization techniques frequently face scalability bottlenecks when dealing with high-dimensional, multi-objective problems, particularly those involving human behavior, uncertainty, and nonlinear system dynamics. In recent years, quantum-inspired optimization (QIO) methods have gained attention for their ability to navigate complex search spaces with improved convergence and global optimality properties. However, their application in user-centric microgrid optimization remains limited, particularly in contexts that require real-time policy adaptation and behavior-aware coordination. To the best of our knowledge, no existing study has proposed a unified framework that jointly integrates QIO, social cognitive modeling, and dynamic incentive mechanisms to address the behavioral and technical complexity of modern microgrids. These limitations highlight the need for a new generation of microgrid optimization strategies—capable of coupling scalable algorithmic search with adaptive, human-centered decision-making. This motivates the hybrid quantum-classical framework proposed in this study.

Mathematical modeling

To formulate the optimization framework for DSM in microgrids, we define a multi-objective problem that integrates SCT with quantum-inspired optimization techniques. The problem formulation consists of decision variables representing energy consumption behaviors, control actions for load scheduling, and incentives for

demand-side participation. The objective functions consider economic cost minimization, peak load reduction, and behavioral adaptation efficiency.

To provide a clear understanding of the variables and parameters involved in the proposed framework, the following nomenclature table presents all essential symbols along with their corresponding definitions and physical units. These symbols are consistently used throughout the modeling and optimization process.

Symbol	Description	Unit
$\Gamma_{i,t}$	Renewable energy generation at node i and time t	MW
$\Lambda_{i,t}$	Load demand at node i and time t	MW
$\Theta_{i,t}$	Economic cost at node i and time t	USD
$\Upsilon_{i,t}$	Environmental impact index at node i and time t	CO ₂ e
$\Psi_{i,t}$	Social acceptance score at node i and time t	score
$\Xi_{k,t}$	Grid resilience metric at node k and time t	unitless
$\Omega_{k,t}$	Stability control index at node k and time t	unitless
$\psi_{m,t}$	Solar energy generation at node m and time t	MW
$\theta_{m,t}$	Wind energy generation at node m and time t	MW
$\rho_{m,t}$	Storage contribution at node m and time t	MW
$\omega_{p,t}$	Curtailement loss at node p and time t	MW
$\pi_{p,t}$	Spillage loss at node p and time t	MW
$\vartheta_{i,t}$	User participation level at time t	score
$\varsigma_{i,t}$	Peer influence factor at time t	score
$\xi_{i,t}$	Self-efficacy score at time t	score
$\zeta_{j,t}$	Gamification engagement factor at time t	score
$\tau_{j,t}$	Direct incentive value at time t	USD
$\Theta_{real_time_control_l,t}$	Real-time control effectiveness at node l and time t	unitless
$\Psi_{forecast_l,t}$	Forecast accuracy metric at node l and time t	unitless
$\Xi_{adaptive_optimization_l,t}$	Adaptive optimization performance at node l and time t	unitless
$\Theta_{fuel_cell_n,t}$	Fuel cell energy generation at node n and time t	MW
$\Psi_{tank_n,t}$	Hydrogen tank storage at node n and time t	MWh
$\Xi_{electrolyzer_n,t}$	Hydrogen dispatch through electrolysis at node n and time t	MWh
$\Theta_{DAC_s,t}$	Direct air capture energy usage at node s and time t	MW
$\Psi_{CCS_s,t}$	Carbon capture and storage at node s and time t	tons CO ₂
$\Xi_{offsets_s,t}$	Carbon trading offsets at node s and time t	tons CO ₂
$\Theta_{industrial_CO2_r,t}$	Industrial emissions at node r and time t	tons CO ₂
$\Psi_{vehicle_emissions_r,t}$	Transport emissions at node r and time t	tons CO ₂

Note: All variables are indexed by space i, j, k, m, n, r, s and time t

To enhance the interpretability of the proposed optimization architecture and respond to reviewer concerns regarding mathematical complexity, a high-level process diagram is presented to illustrate the overall framework. This visualization provides an intuitive overview of the layered components and information flow in the quantum-classical hybrid optimization process.

As shown in Fig. 1, the optimization process begins with data collection on microgrid structure, user profiles, and external signals. This is followed by encoding behavior-based features using Social Cognitive Theory (SCT). The core multi-objective dispatch problem is then solved through a quantum-inspired optimization layer, aiming to balance cost, carbon emissions, and behavioral participation. The resulting strategy is translated into implementable pricing and incentive signals. Finally, the system's performance is evaluated via simulation, comparing economic, environmental, and behavioral metrics. This layered workflow improves clarity and bridges the gap between mathematical formulation and practical interpretation.

$$\min_{\pi, \kappa, \theta, \xi} \sum_{t=1}^T \sum_{i \in \mathcal{N}} \left(\alpha_t^{\text{cap}} \cdot \varphi_{i,t} + \beta_{\psi}^{\text{op}} \cdot \omega_{i,t} + \gamma_{\tau}^{\text{sub}} \cdot \chi_{i,t} \right) + \sum_{t=1}^T \sum_{j \in \mathcal{M}} \left(\delta_{\sigma}^{\text{maint}} \cdot \lambda_{j,t} + \zeta_{\rho}^{\text{pen}} \cdot v_{j,t} \right) \quad (1)$$

One of the cornerstones of an economically viable microgrid is cost efficiency, which is intricately embedded into this objective function. Here, the life-cycle cost minimization accounts for several major economic components: the capital investment cost α_t^{cap} multiplied by the allocated infrastructure capacity $\varphi_{i,t}$, the operational expenditure β_{ψ}^{op} linked with the real-time operational power $\omega_{i,t}$, and the impact of subsidies $\gamma_{\tau}^{\text{sub}}$ adjusting the financial balance through $\chi_{i,t}$. Moreover, long-term financial sustainability is ensured through maintenance costs $\delta_{\sigma}^{\text{maint}}$ weighted against the degradation $\lambda_{j,t}$ of energy storage and infrastructure, while penalties for inefficiency $\zeta_{\rho}^{\text{pen}}$ penalize poor performance through $v_{j,t}$. The entire function spans multiple spatial nodes i and temporal periods t , ensuring a holistic and granular cost analysis.

$$\max_{\alpha, \beta, \gamma} \sum_{t=1}^T \sum_{m \in \mathcal{R}} \left(\lambda_{\phi}^{\text{sol}} \cdot \psi_{m,t} + \mu_{\zeta}^{\text{wind}} \cdot \theta_{m,t} + \nu_{\eta}^{\text{stor}} \cdot \rho_{m,t} \right) - \sum_{t=1}^T \sum_{p \in \mathcal{D}} \left(\sigma_{\chi}^{\text{curt}} \cdot \omega_{p,t} + \tau_{\kappa}^{\text{spillage}} \cdot \pi_{p,t} \right) \quad (2)$$

Maximizing the utilization of renewable energy resources is pivotal for sustainability. This function captures the total contribution of solar, wind, and hybrid storage in the microgrid, weighted by their respective efficiency factors $\lambda_{\phi}^{\text{sol}}$, $\mu_{\zeta}^{\text{wind}}$, ν_{η}^{stor} . However, energy is not always fully utilized; curtailment $\sigma_{\chi}^{\text{curt}}$ and spillage $\tau_{\kappa}^{\text{spillage}}$ reduce overall efficiency. By subtracting these losses from the renewable energy generation, the model ensures that the microgrid prioritizes clean energy sources, optimally balancing generation and storage utilization over time t and regions m .

$$\max_{\omega, \theta, \psi, \chi} \sum_{t=1}^T \sum_{i \in \mathcal{U}} \left(\omega_{\alpha}^{\text{part}} \cdot \vartheta_{i,t} + \theta_{\beta}^{\text{peer}} \cdot \varsigma_{i,t} + \psi_{\gamma}^{\text{self}} \cdot \xi_{i,t} \right) + \sum_{t=1}^T \sum_{j \in \mathcal{Q}} \left(\chi_{\delta}^{\text{game}} \cdot \zeta_{j,t} + \kappa_{\epsilon}^{\text{incent}} \cdot \tau_{j,t} \right) \quad (3)$$

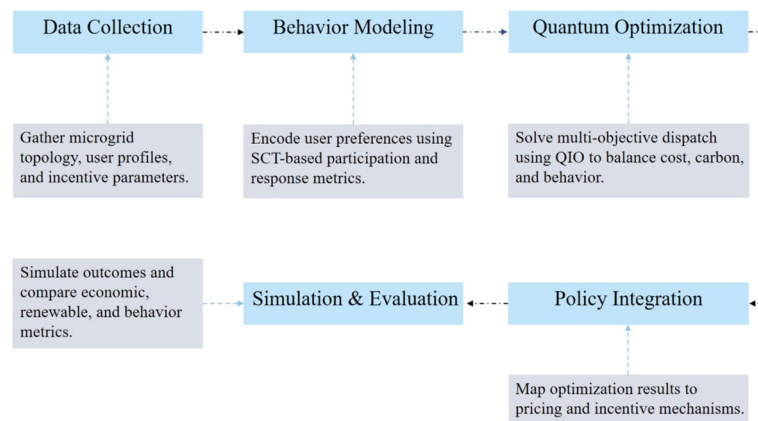


Fig. 1. Workflow of the proposed behavior-aware energy management framework.

User engagement is a key enabler of microgrid sustainability, and this function prioritizes demand response participation through a behavioral incentive structure. The participation level $\vartheta_{i,t}$ is influenced by peer influence $\varsigma_{i,t}$, self-efficacy $\xi_{i,t}$, gamification-driven engagement $\zeta_{j,t}$, and direct financial incentives $\tau_{j,t}$. Coefficients $\omega_{\alpha}^{\text{part}}, \theta_{\beta}^{\text{peer}}, \psi_{\gamma}^{\text{self}}$ capture the behavioral impact of social cognitive factors, while $\chi_{\delta}^{\text{game}}, \kappa_{\varepsilon}^{\text{incent}}$ reflect financial and psychological motivators. This multi-dimensional function ensures optimal design of behavioral mechanisms to maximize voluntary user participation.

$$\min_{\Phi, \Omega, \Lambda} \sum_{t=1}^T \sum_{i \in \mathcal{S}} \left(\Phi_{\alpha}^{\text{econ}} \cdot \Theta_{i,t} + \Omega_{\beta}^{\text{env}} \cdot \Upsilon_{i,t} + \Lambda_{\gamma}^{\text{social}} \cdot \Psi_{i,t} \right) + \sum_{t=1}^T \sum_{k \in \mathcal{D}} \left(\Xi_{\delta}^{\text{resil}} \cdot \Omega_{k,t} + \Psi_{\varepsilon}^{\text{stability}} \cdot \Lambda_{k,t} \right) \quad (4)$$

A multi-objective trade-off function is essential to balance economic, environmental, and social goals while ensuring grid resilience and stability. Economic costs $\Theta_{i,t}$, environmental impact $\Upsilon_{i,t}$, and social acceptance $\Psi_{i,t}$ are assigned appropriate weights $\Phi_{\alpha}^{\text{econ}}, \Omega_{\beta}^{\text{env}}, \Lambda_{\gamma}^{\text{social}}$ to capture the trade-offs among competing priorities. Resilience $\Omega_{k,t}$ and stability $\Lambda_{k,t}$ factors are also included to ensure that the microgrid can withstand operational uncertainties. This formulation enables a holistic optimization approach that does not favor one aspect at the expense of another, resulting in a well-rounded decision-making framework.

$$\sum_{t=1}^T \sum_{i \in \mathcal{N}} \left(\Psi_{\alpha}^{\text{gen}} \cdot \Gamma_{i,t} - \Omega_{\beta}^{\text{demand}} \cdot \Lambda_{i,t} + \Xi_{\gamma}^{\text{storage}} \cdot \Upsilon_{i,t} \right) + \sum_{t=1}^T \sum_{j \in \mathcal{M}} \left(\Phi_{\delta}^{\text{dispatch}} \cdot \Theta_{j,t} + \Omega_{\varepsilon}^{\text{curtailment}} \cdot \Xi_{j,t} - \Lambda_{\zeta}^{\text{reserve}} \cdot \Psi_{j,t} \right) = 0 \quad (5)$$

Energy balance must be maintained across the entire microgrid, ensuring that generation, storage, and dispatch are harmonized with demand, curtailment, and reserve allocation. The first term $\Psi_{\alpha}^{\text{gen}} \cdot \Gamma_{i,t}$ represents total power generation from all renewable sources, weighted by efficiency $\Psi_{\alpha}^{\text{gen}}$. The demand-side requirement $\Omega_{\beta}^{\text{demand}} \cdot \Lambda_{i,t}$ subtracts the consumption load, ensuring that at any time step t , supply aligns with demand. The energy storage dynamics are captured through $\Xi_{\gamma}^{\text{storage}} \cdot \Upsilon_{i,t}$, allowing surplus power to be preserved for future use. Additionally, dispatchable resources $\Phi_{\delta}^{\text{dispatch}} \cdot \Theta_{j,t}$ provide supplementary energy, while curtailment $\Omega_{\varepsilon}^{\text{curtailment}} \cdot \Xi_{j,t}$ ensures grid stability by limiting excess inflows. Finally, the reserve constraint $\Lambda_{\zeta}^{\text{reserve}} \cdot \Psi_{j,t}$ guarantees that emergency power is set aside for contingencies. By summing these terms over all spatial nodes \mathcal{N} and microgrid segments \mathcal{M} , this constraint ensures that energy flows within the system are consistently balanced.

$$\sum_{t=1}^T \sum_{i \in \mathcal{R}} \left(\Lambda_{\alpha}^{\text{wind}} \cdot \Xi_{i,t}^{\text{wind}} + \Omega_{\beta}^{\text{solar}} \cdot \Psi_{i,t}^{\text{solar}} + \Phi_{\gamma}^{\text{hydro}} \cdot \Theta_{i,t}^{\text{hydro}} \right) - \sum_{t=1}^T \sum_{j \in \mathcal{D}} \left(\Phi_{\delta}^{\text{curt}} \cdot \Xi_{j,t}^{\text{curt}} + \Psi_{\varepsilon}^{\text{spill}} \cdot \Omega_{j,t}^{\text{spill}} \right) \leq \Phi_{\zeta}^{\text{avail}} \quad (6)$$

Renewable energy generation is inherently uncertain and subject to natural variability. This constraint ensures that the combined wind, solar, and hydro power generation does not exceed the system's upper operational capacity $\Phi_{\zeta}^{\text{avail}}$. Each energy source—wind $\Lambda_{\alpha}^{\text{wind}} \cdot \Xi_{i,t}^{\text{wind}}$, solar $\Omega_{\beta}^{\text{solar}} \cdot \Psi_{i,t}^{\text{solar}}$, and hydro $\Phi_{\gamma}^{\text{hydro}} \cdot \Theta_{i,t}^{\text{hydro}}$

—contributes to the overall generation, while energy losses due to curtailment $\Phi_{\delta}^{\text{curt}} \cdot \Xi_{j,t}^{\text{curt}}$ and spillage $\Psi_{\varepsilon}^{\text{spill}} \cdot \Omega_{j,t}^{\text{spill}}$ reduce net availability. This constraint ensures that the total renewable power utilized remains within system limits while minimizing energy waste.

$$\sum_{t=1}^T \sum_{k \in \mathcal{S}} \left(\Lambda_{\alpha}^{\text{charge}} \cdot \Theta_{k,t}^{\text{charge}} - \Omega_{\beta}^{\text{discharge}} \cdot \Xi_{k,t}^{\text{discharge}} \right) + \sum_{t=1}^T \sum_{j \in \mathcal{D}} \left(\Phi_{\gamma}^{\text{degrade}} \cdot \Psi_{j,t}^{\text{degrade}} \right) \leq \Phi_{\zeta}^{\text{stor-cap}} \quad (7)$$

Storage capacity is fundamental to balancing energy supply and demand. The stored energy is increased through charging $\Lambda_{\alpha}^{\text{charge}} \cdot \Theta_{k,t}^{\text{charge}}$ and depleted by discharging $\Omega_{\beta}^{\text{discharge}} \cdot \Xi_{k,t}^{\text{discharge}}$. However, battery degradation is inevitable and captured through $\Phi_{\gamma}^{\text{degrade}} \cdot \Psi_{j,t}^{\text{degrade}}$, ensuring the system accounts for capacity loss over time. The right-hand side ensures that total energy stored does not exceed the physical capacity $\Phi_{\zeta}^{\text{stor-cap}}$.

$$\sum_{t=1}^T \sum_{m \in \mathcal{Q}} \left(\Lambda_{\alpha}^{\text{voltage}} \cdot \Xi_{m,t}^V + \Omega_{\beta}^{\text{frequency}} \cdot \Psi_{m,t}^f + \Phi_{\gamma}^{\text{stability}} \cdot \Theta_{m,t}^{\text{stab}} \right) \geq \Phi_{\zeta}^{\text{safe}} \quad (8)$$

Grid stability requires maintaining voltage, frequency, and overall system balance. The voltage level $\Lambda_{\alpha}^{\text{voltage}} \cdot \Xi_{m,t}^V$ must remain within permissible limits, frequency deviations $\Omega_{\beta}^{\text{frequency}} \cdot \Psi_{m,t}^f$ should be minimized, and overall stability $\Phi_{\gamma}^{\text{stability}} \cdot \Theta_{m,t}^{\text{stab}}$ needs to be assured. This constraint ensures that these operational parameters always meet or exceed a predefined safety threshold $\Phi_{\zeta}^{\text{safe}}$, guaranteeing reliable microgrid operation.

$$\sum_{t=1}^T \sum_{j \in \mathcal{R}} \left(\Lambda_{\alpha}^{\text{policy}} \cdot \Xi_{j,t}^{\text{subsidy}} + \Omega_{\beta}^{\text{incent}} \cdot \Psi_{j,t}^{\text{rebate}} + \Phi_{\gamma}^{\text{tariff}} \cdot \Theta_{j,t}^{\text{tariff}} \right) \leq \Phi_{\zeta}^{\text{budget}} \quad (9)$$

A robust policy framework is necessary to promote renewable energy adoption and ensure financial sustainability. The subsidy allocation $\Lambda_{\alpha}^{\text{policy}} \cdot \Xi_{j,t}^{\text{subsidy}}$, incentive rebates $\Omega_{\beta}^{\text{incent}} \cdot \Psi_{j,t}^{\text{rebate}}$, and tariff adjustments $\Phi_{\gamma}^{\text{tariff}} \cdot \Theta_{j,t}^{\text{tariff}}$ are capped within a predefined policy budget $\Phi_{\zeta}^{\text{budget}}$. This constraint ensures that financial incentives are optimally distributed without exceeding fiscal limitations.

$$\sum_{t=1}^T \sum_{i \in \mathcal{G}} \left(\Lambda_{\alpha}^{\text{co2}} \cdot \Xi_{i,t}^{\text{emit}} - \Omega_{\beta}^{\text{offset}} \cdot \Psi_{i,t}^{\text{capture}} \right) \leq \Phi_{\zeta}^{\text{limit}} \quad (10)$$

Reducing carbon emissions is a central sustainability goal. This constraint ensures that total emissions $\Lambda_{\alpha}^{\text{co2}} \cdot \Xi_{i,t}^{\text{emit}}$ do not exceed allowable limits $\Phi_{\zeta}^{\text{limit}}$, while accounting for carbon capture mechanisms $\Omega_{\beta}^{\text{offset}} \cdot \Psi_{i,t}^{\text{capture}}$ that mitigate environmental impact.

$$\sum_{t=1}^T \sum_{i \in \mathcal{L}} \left(\Theta_{\alpha}^{\text{demand_response}} \cdot \Xi_{i,t}^{\text{shift}} + \Omega_{\beta}^{\text{flex}} \cdot \Psi_{i,t}^{\text{reduction}} + \Phi_{\gamma}^{\text{game}} \cdot \Lambda_{i,t}^{\text{participation}} \right) \geq \Phi_{\zeta}^{\text{engagement}} \quad (11)$$

Demand-side flexibility is crucial for ensuring grid stability and reducing reliance on non-renewable energy sources. This equation establishes a lower bound for user engagement in demand response programs. The first term $\Theta_{\alpha}^{\text{demand_response}} \cdot \Xi_{i,t}^{\text{shift}}$ quantifies the power shifted from peak to off-peak hours through automated scheduling, reducing the need for additional generation. The second component, $\Omega_{\beta}^{\text{flex}} \cdot \Psi_{i,t}^{\text{reduction}}$, captures voluntary load reductions driven by real-time price signals and behavioral nudges. Lastly, the effect of gamification $\Phi_{\gamma}^{\text{game}} \cdot \Lambda_{i,t}^{\text{participation}}$ ensures that engagement remains high through incentive-based programs. This equation sets a minimum engagement level $\Phi_{\zeta}^{\text{engagement}}$ to guarantee that enough users actively participate in demand flexibility schemes.

$$\sum_{t=1}^T \sum_{m \in \mathcal{K}} \left(\Lambda_{\alpha}^{\text{cyber}} \cdot \Theta_{m,t}^{\text{attack}} + \Omega_{\beta}^{\text{resilience}} \cdot \Psi_{m,t}^{\text{recovery}} + \Phi_{\gamma}^{\text{redundancy}} \cdot \Xi_{m,t}^{\text{backup}} \right) \leq \Phi_{\zeta}^{\text{risk}} \quad (12)$$

With increasing digitalization of energy systems, microgrids are vulnerable to cyberattacks. This constraint ensures that the total cyber risk remains within an acceptable threshold $\Phi_{\zeta}^{\text{risk}}$. The first term $\Lambda_{\alpha}^{\text{cyber}} \cdot \Theta_{m,t}^{\text{attack}}$ represents potential cyber threats targeting the system. Resilience mechanisms $\Omega_{\beta}^{\text{resilience}} \cdot \Psi_{m,t}^{\text{recovery}}$ allow rapid system recovery after an attack, mitigating its impact. The backup power and redundancy factor $\Phi_{\gamma}^{\text{redundancy}} \cdot \Xi_{m,t}^{\text{backup}}$ ensures that alternative paths and backup systems maintain continuity of service, reducing cyber-induced power disruptions.

$$\sum_{t=1}^T \sum_{j \in \mathcal{R}} \left(\Lambda_{\alpha}^{\text{tariff}} \cdot \Theta_{j,t}^{\text{real_time}} + \Omega_{\beta}^{\text{subsidy}} \cdot \Psi_{j,t}^{\text{dynamic}} + \Phi_{\gamma}^{\text{fair}} \cdot \Xi_{j,t}^{\text{equity}} \right) \geq \Phi_{\zeta}^{\text{affordability}} \quad (13)$$

Electricity pricing structures influence energy consumption behaviors and must balance affordability with economic sustainability. This equation ensures that real-time tariffs $\Lambda_{\alpha}^{\text{tariff}} \cdot \Theta_{j,t}^{\text{real_time}}$, dynamic subsidies $\Omega_{\beta}^{\text{subsidy}} \cdot \Psi_{j,t}^{\text{dynamic}}$, and fair pricing mechanisms $\Phi_{\gamma}^{\text{fair}} \cdot \Xi_{j,t}^{\text{equity}}$ collectively maintain an acceptable affordability level $\Phi_{\zeta}^{\text{affordability}}$. It guarantees that financial burdens are not disproportionately placed on low-income users while still maintaining revenue streams for grid operators.

$$\sum_{t=1}^T \sum_{p \in \mathcal{V}} \left(\Lambda_{\alpha}^{\text{electric_vehicle}} \cdot \Theta_{p,t}^{\text{charge}} - \Omega_{\beta}^{\text{discharge}} \cdot \Psi_{p,t}^{\text{V2G}} \right) \leq \Phi_{\zeta}^{\text{grid_impact}} \quad (14)$$

Electric vehicles (EVs) present both opportunities and challenges for microgrid operation. While EVs can store and supply energy through vehicle-to-grid (V2G) mechanisms, uncoordinated charging could stress the grid. This constraint ensures that charging $\Lambda_{\alpha}^{\text{electric_vehicle}} \cdot \Theta_{p,t}^{\text{charge}}$ and discharging through V2G $\Omega_{\beta}^{\text{discharge}} \cdot \Psi_{p,t}^{\text{V2G}}$ remain within grid stability limits $\Phi_{\zeta}^{\text{grid_impact}}$. Optimally managing EV energy flows is key to leveraging them as distributed energy resources.

$$\sum_{t=1}^T \sum_{q \in \mathcal{W}} \left(\Lambda_{\alpha}^{\text{microgrid}} \cdot \Theta_{q,t}^{\text{grid_tie}} + \Omega_{\beta}^{\text{island}} \cdot \Psi_{q,t}^{\text{self_suff}} \right) \geq \Phi_{\zeta}^{\text{resilience}} \quad (15)$$

Microgrids operate in either grid-connected or islanded mode. During grid outages, the system must maintain self-sufficiency. This equation ensures that total available power from grid connections $\Lambda_{\alpha}^{\text{microgrid}} \cdot \Theta_{q,t}^{\text{grid_tie}}$ and islanded microgrid operations $\Omega_{\beta}^{\text{island}} \cdot \Psi_{q,t}^{\text{self_suff}}$ remain above a resilience threshold $\Phi_{\zeta}^{\text{resilience}}$. This guarantees operational continuity, even in extreme conditions.

$$\sum_{t=1}^T \sum_{r \in \mathcal{R}} \left(\Lambda_{\alpha}^{\text{social_impact}} \cdot \Theta_{r,t}^{\text{acceptance}} + \Omega_{\beta}^{\text{behavior}} \cdot \Psi_{r,t}^{\text{peer_effect}} + \Phi_{\gamma}^{\text{education}} \cdot \Xi_{r,t}^{\text{awareness}} \right) \geq \Phi_{\zeta}^{\text{adoption}} \quad (16)$$

Behavioral adoption of microgrid solutions is as critical as technical and economic feasibility. This constraint ensures that the social impact of microgrid adoption remains significant. Public acceptance $\Lambda_{\alpha}^{\text{social_impact}} \cdot \Theta_{r,t}^{\text{acceptance}}$, peer influence $\Omega_{\beta}^{\text{behavior}} \cdot \Psi_{r,t}^{\text{peer_effect}}$, and energy literacy $\Phi_{\gamma}^{\text{education}} \cdot \Xi_{r,t}^{\text{awareness}}$ all contribute to a required level of sustainable technology adoption $\Phi_{\zeta}^{\text{adoption}}$. This function ensures that technological advances align with social norms and user engagement strategies.

$$\sum_{t=1}^T \sum_{s \in \mathcal{S}} \left(\Lambda_{\alpha}^{\text{power_flow}} \cdot \Theta_{s,t}^{\text{Kirchhoff}} + \Omega_{\beta}^{\text{network_stability}} \cdot \Psi_{s,t}^{\text{load_balance}} \right) \leq \Phi_{\zeta}^{\text{grid_safety}} \quad (17)$$

The integrity of the microgrid's electrical network is governed by Kirchhoff's laws and load balancing mechanisms. Ensuring safe and reliable operation requires maintaining voltage and power flow stability. This equation restricts deviations by ensuring Kirchhoff's current law (KCL) compliance $\Lambda_{\alpha}^{\text{power_flow}} \cdot \Theta_{s,t}^{\text{Kirchhoff}}$ and network-wide stability $\Omega_{\beta}^{\text{network_stability}} \cdot \Psi_{s,t}^{\text{load_balance}}$ within acceptable operational thresholds $\Phi_{\zeta}^{\text{grid_safety}}$. This guarantees efficient energy transmission without overload risks.

$$\begin{aligned} & \sum_{t=1}^T \sum_{i \in \mathcal{B}} \left(\Lambda_{\alpha}^{\text{thermal_storage}} \cdot \Theta_{i,t}^{\text{heat_storage}} + \Omega_{\beta}^{\text{co_generation}} \cdot \Psi_{i,t}^{\text{CHP}} + \Phi_{\gamma}^{\text{heat_recovery}} \cdot \Xi_{i,t}^{\text{recovered_heat}} \right) \\ & - \sum_{t=1}^T \sum_{j \in \mathcal{H}} \left(\Lambda_{\delta}^{\text{heat_demand}} \cdot \Theta_{j,t}^{\text{load}} + \Omega_{\epsilon}^{\text{heat_loss}} \cdot \Psi_{j,t}^{\text{transmission_loss}} \right) \geq 0 \end{aligned} \quad (18)$$

Efficient heat management is crucial in microgrids integrating combined heat and power (CHP) systems. This equation ensures that total available thermal energy from storage $\Lambda_{\alpha}^{\text{thermal_storage}} \cdot \Theta_{i,t}^{\text{heat_storage}}$, CHP generation $\Omega_{\beta}^{\text{co_generation}} \cdot \Psi_{i,t}^{\text{CHP}}$, and recovered waste heat $\Phi_{\gamma}^{\text{heat_recovery}} \cdot \Xi_{i,t}^{\text{recovered_heat}}$ is sufficient to meet heating demand $\Lambda_{\delta}^{\text{heat_demand}} \cdot \Theta_{j,t}^{\text{load}}$ while accounting for losses $\Omega_{\epsilon}^{\text{heat_loss}} \cdot \Psi_{j,t}^{\text{transmission_loss}}$. This ensures thermal energy sustainability while minimizing waste.

$$\begin{aligned} & \sum_{t=1}^T \sum_{m \in \mathcal{F}} \left(\Lambda_{\alpha}^{\text{water_supply}} \cdot \Theta_{m,t}^{\text{reservoir}} + \Omega_{\beta}^{\text{desalination}} \cdot \Psi_{m,t}^{\text{RO_process}} + \Phi_{\gamma}^{\text{wastewater_reuse}} \cdot \Xi_{m,t}^{\text{treatment}} \right) \\ & - \sum_{t=1}^T \sum_{p \in \mathcal{P}} \left(\Lambda_{\delta}^{\text{water_demand}} \cdot \Theta_{p,t}^{\text{consumption}} + \Omega_{\epsilon}^{\text{evaporation}} \cdot \Psi_{p,t}^{\text{loss}} \right) \geq 0 \end{aligned} \quad (19)$$

Water-energy nexus is critical in microgrid operations, especially for sustainable communities. This equation ensures a balance between available water supply from reservoirs $\Lambda_{\alpha}^{\text{water_supply}} \cdot \Theta_{m,t}^{\text{reservoir}}$, desalination $\Omega_{\beta}^{\text{desalination}} \cdot \Psi_{m,t}^{\text{RO_process}}$, and treated wastewater $\Phi_{\gamma}^{\text{wastewater_reuse}} \cdot \Xi_{m,t}^{\text{treatment}}$, against the water demand $\Lambda_{\delta}^{\text{water_demand}} \cdot \Theta_{p,t}^{\text{consumption}}$ and evaporation losses $\Omega_{\epsilon}^{\text{evaporation}} \cdot \Psi_{p,t}^{\text{loss}}$. This constraint supports sustainable water management in microgrids.

$$\begin{aligned}
& \sum_{t=1}^T \sum_{q \in \mathcal{Q}} \left(\Lambda_{\alpha}^{\text{grid_reconfig}} \cdot \Theta_{q,t}^{\text{switch_status}} + \Omega_{\beta}^{\text{fault_isolation}} \cdot \Psi_{q,t}^{\text{contingency}} \right. \\
& \quad \left. + \Phi_{\gamma}^{\text{self_healing}} \cdot \Xi_{q,t}^{\text{autonomous_correction}} \right) \\
& - \sum_{t=1}^T \sum_{s \in \mathcal{C}} \left(\Lambda_{\delta}^{\text{outage_impact}} \cdot \Theta_{s,t}^{\text{disruption}} + \Omega_{\varepsilon}^{\text{restoration_delay}} \cdot \Psi_{s,t}^{\text{time}} \right) \geq 0
\end{aligned} \tag{20}$$

Microgrid resilience under fault scenarios requires dynamic network reconfiguration and self-healing capabilities. This equation ensures that grid reconfiguration $\Lambda_{\alpha}^{\text{grid_reconfig}} \cdot \Theta_{q,t}^{\text{switch_status}}$, fault isolation strategies $\Omega_{\beta}^{\text{fault_isolation}} \cdot \Psi_{q,t}^{\text{contingency}}$, and autonomous self-healing mechanisms $\Phi_{\gamma}^{\text{self_healing}} \cdot \Xi_{q,t}^{\text{autonomous_correction}}$ effectively mitigate power outages $\Lambda_{\delta}^{\text{outage_impact}} \cdot \Theta_{s,t}^{\text{disruption}}$ and reduce restoration delays $\Omega_{\varepsilon}^{\text{restoration_delay}} \cdot \Psi_{s,t}^{\text{time}}$. This constraint ensures that microgrid stability is preserved under disturbances.

$$\begin{aligned}
& \sum_{t=1}^T \sum_{l \in \mathcal{M}} \left(\Lambda_{\alpha}^{\text{AI_dispatch}} \cdot \Theta_{l,t}^{\text{real_time_control}} \right. \\
& \quad \left. + \Omega_{\beta}^{\text{predictive_modeling}} \cdot \Psi_{l,t}^{\text{forecast}} + \Phi_{\gamma}^{\text{multi_objective_learning}} \cdot \Xi_{l,t}^{\text{adaptive_optimization}} \right) \geq \Phi_{\zeta}^{\text{efficiency}}
\end{aligned} \tag{21}$$

Advanced artificial intelligence (AI) and machine learning techniques are crucial for optimizing microgrid operations in real time. This constraint ensures that AI-driven real-time dispatch $\Lambda_{\alpha}^{\text{AI_dispatch}} \cdot \Theta_{l,t}^{\text{real_time_control}}$, predictive modeling $\Omega_{\beta}^{\text{predictive_modeling}} \cdot \Psi_{l,t}^{\text{forecast}}$, and adaptive multi-objective learning $\Phi_{\gamma}^{\text{multi_objective_learning}} \cdot \Xi_{l,t}^{\text{adaptive_optimization}}$ meet the minimum operational efficiency standard $\Phi_{\zeta}^{\text{smart_grid_efficiency}}$. This ensures smart decision-making for grid operation and resource allocation.

$$\begin{aligned}
& \sum_{t=1}^T \sum_{n \in \mathcal{Z}} \left(\Lambda_{\alpha}^{\text{hydrogen_integration}} \cdot \Theta_{n,t}^{\text{fuel_cell}} \right. \\
& \quad \left. + \Omega_{\beta}^{\text{hydrogen_storage}} \cdot \Psi_{n,t}^{\text{tank}} + \Phi_{\gamma}^{\text{hydrogen_dispatch}} \cdot \Xi_{n,t}^{\text{electrolyzer}} \right) \geq \Phi_{\zeta}^{\text{H2_supply}}
\end{aligned} \tag{22}$$

Hydrogen-based energy storage and fuel cell integration are emerging solutions for microgrid sustainability. This equation ensures that hydrogen fuel cell generation $\Lambda_{\alpha}^{\text{hydrogen_integration}} \cdot \Theta_{n,t}^{\text{fuel_cell}}$, hydrogen storage in tanks $\Omega_{\beta}^{\text{hydrogen_storage}} \cdot \Psi_{n,t}^{\text{tank}}$, and electrolysis-based hydrogen dispatch $\Phi_{\gamma}^{\text{hydrogen_dispatch}} \cdot \Xi_{n,t}^{\text{electrolyzer}}$ remain sufficient to meet the hydrogen demand requirement $\Phi_{\zeta}^{\text{H2_supply}}$. This facilitates the integration of green hydrogen into microgrid energy systems.

$$\begin{aligned}
& \sum_{t=1}^T \sum_{s \in \mathcal{E}} \left(\Lambda_{\alpha}^{\text{carbon_sequestration}} \cdot \Theta_{s,t}^{\text{DAC}} + \Omega_{\beta}^{\text{carbon_storage}} \cdot \Psi_{s,t}^{\text{CCS}} + \Phi_{\gamma}^{\text{carbon_trading}} \cdot \Xi_{s,t}^{\text{offsets}} \right) \\
& - \sum_{t=1}^T \sum_{r \in \mathcal{G}} \left(\Lambda_{\delta}^{\text{carbon_emission}} \cdot \Theta_{r,t}^{\text{industrial_CO2}} + \Omega_{\varepsilon}^{\text{transport_CO2}} \cdot \Psi_{r,t}^{\text{vehicle_emissions}} \right) \leq 0
\end{aligned} \tag{23}$$

Carbon neutrality is an essential component of sustainable microgrid operations, necessitating active carbon capture and mitigation strategies. This equation ensures that total carbon sequestration from direct air capture (DAC) $\Lambda_{\alpha}^{\text{carbon_sequestration}} \cdot \Theta_{s,t}^{\text{DAC}}$, carbon capture and storage (CCS) $\Omega_{\beta}^{\text{carbon_storage}} \cdot \Psi_{s,t}^{\text{CCS}}$, and carbon credit trading $\Phi_{\gamma}^{\text{carbon_trading}} \cdot \Xi_{s,t}^{\text{offsets}}$ effectively neutralize carbon emissions from industrial sources $\Lambda_{\delta}^{\text{carbon_emission}} \cdot \Theta_{r,t}^{\text{industrial_CO2}}$ and transport-related emissions $\Omega_{\varepsilon}^{\text{transport_CO2}} \cdot \Psi_{r,t}^{\text{vehicle_emissions}}$. This constraint ensures that the microgrid maintains a net-zero carbon balance.

$$\begin{aligned}
& \sum_{t=1}^T \sum_{q \in \mathcal{Q}} \left(\Lambda_{\alpha}^{\text{blockchain_transactions}} \cdot \Theta_{q,t}^{\text{energy_trading}} \right. \\
& \quad \left. + \Omega_{\beta}^{\text{peer_to_peer}} \cdot \Psi_{q,t}^{\text{decentralized_market}} + \Phi_{\gamma}^{\text{contract_enforcement}} \cdot \Xi_{q,t}^{\text{smart_contracts}} \right) \\
& - \sum_{t=1}^T \sum_{w \in \mathcal{W}} \left(\Lambda_{\delta}^{\text{market_volatility}} \cdot \Theta_{w,t}^{\text{price_fluctuation}} \right. \\
& \quad \left. + \Omega_{\varepsilon}^{\text{transaction_fees}} \cdot \Psi_{w,t}^{\text{costs}} \right) \geq \Phi_{\zeta}^{\text{market_stability}}
\end{aligned} \tag{24}$$

Decentralized energy markets enabled by blockchain technology enhance transaction efficiency, but market stability must be ensured. This equation ensures that total decentralized trading activities—blockchain-based energy transactions $\Lambda_{\alpha}^{\text{blockchain_transactions}} \cdot \Theta_{q,t}^{\text{energy_trading}}$, peer-to-peer energy exchange $\Omega_{\beta}^{\text{peer_to_peer}} \cdot \Psi_{q,t}^{\text{decentralized_market}}$, and smart contract automation $\Phi_{\gamma}^{\text{contract_enforcement}} \cdot \Xi_{q,t}^{\text{smart_contracts}}$ —counteract the effects of price volatility $\Lambda_{\delta}^{\text{market_volatility}} \cdot \Theta_{w,t}^{\text{price_fluctuation}}$ and transaction fees $\Omega_{\varepsilon}^{\text{transaction_fees}} \cdot \Psi_{w,t}^{\text{costs}}$, maintaining a stable and efficient microgrid energy market.

$$\begin{aligned}
& \sum_{t=1}^T \sum_{v \in \mathcal{V}} \left(\Lambda_{\alpha}^{\text{waste_to_energy}} \cdot \Theta_{v,t}^{\text{biogas}} \right. \\
& \quad \left. + \Omega_{\beta}^{\text{recycling_efficiency}} \cdot \Psi_{v,t}^{\text{material_recovery}} + \Phi_{\gamma}^{\text{composting}} \cdot \Xi_{v,t}^{\text{organic_waste}} \right) \\
& - \sum_{t=1}^T \sum_{z \in \mathcal{Z}} \left(\Lambda_{\delta}^{\text{landfill_waste}} \cdot \Theta_{z,t}^{\text{solid_waste}} \right. \\
& \quad \left. + \Omega_{\varepsilon}^{\text{GHG_from_waste}} \cdot \Psi_{z,t}^{\text{methane}} \right) \geq \Phi_{\zeta}^{\text{circular_economy}}
\end{aligned} \tag{25}$$

A sustainable microgrid must incorporate a circular economy approach to waste management. This equation ensures that waste-to-energy conversion $\Lambda_{\alpha}^{\text{waste_to_energy}} \cdot \Theta_{v,t}^{\text{biogas}}$, improved recycling $\Omega_{\beta}^{\text{recycling_efficiency}} \cdot \Psi_{v,t}^{\text{material_recovery}}$, and composting $\Phi_{\gamma}^{\text{composting}} \cdot \Xi_{v,t}^{\text{organic_waste}}$ counterbalance landfill waste $\Lambda_{\delta}^{\text{landfill_waste}} \cdot \Theta_{z,t}^{\text{solid_waste}}$ and methane emissions $\Omega_{\varepsilon}^{\text{GHG_from_waste}} \cdot \Psi_{z,t}^{\text{methane}}$. This ensures that microgrid operations contribute to a zero-waste, circular economy.

$$\begin{aligned}
& \sum_{t=1}^T \sum_{u \in \mathcal{U}} \left(\Lambda_{\alpha}^{\text{quantum_annealing}} \cdot \Theta_{u,t}^{\text{optimization_state}} \right. \\
& \quad \left. + \Omega_{\beta}^{\text{quantum_tunneling}} \cdot \Psi_{u,t}^{\text{energy_barrier}} + \Phi_{\gamma}^{\text{quantum_entanglement}} \cdot \Xi_{u,t}^{\text{correlated_states}} \right) \\
& - \sum_{t=1}^T \sum_{y \in \mathcal{Y}} \left(\Lambda_{\delta}^{\text{classical_limitation}} \cdot \Theta_{y,t}^{\text{computational_cost}} \right. \\
& \quad \left. + \Omega_{\varepsilon}^{\text{uncertainty_noise}} \cdot \Psi_{y,t}^{\text{quantum_error}} \right) \geq \Phi_{\zeta}^{\text{quantum_advantage}}
\end{aligned} \tag{26}$$

The integration of QIO into microgrid management ensures computational efficiency in solving large-scale, multi-objective problems. This equation models how quantum annealing $\Lambda_{\alpha}^{\text{quantum_annealing}} \cdot \Theta_{u,t}^{\text{optimization_state}}$, quantum tunneling $\Omega_{\beta}^{\text{quantum_tunneling}} \cdot \Psi_{u,t}^{\text{energy_barrier}}$, and quantum entanglement $\Phi_{\gamma}^{\text{quantum_entanglement}} \cdot \Xi_{u,t}^{\text{correlated_states}}$ improve solution search efficiency compared to classical optimization approaches. These quantum properties must offset computational limitations $\Lambda_{\delta}^{\text{classical_limitation}} \cdot \Theta_{y,t}^{\text{computational_cost}}$ and quantum error noise $\Omega_{\varepsilon}^{\text{uncertainty_noise}} \cdot \Psi_{y,t}^{\text{quantum_error}}$ to achieve a quantum advantage threshold $\Phi_{\zeta}^{\text{quantum_advantage}}$, ensuring the practical feasibility of QIO in real-world microgrid applications.

$$\begin{aligned}
& \sum_{t=1}^T \sum_{c \in \mathcal{O}} \left(\Lambda_{\alpha}^{\text{social_learning}} \cdot \Theta_{c,t}^{\text{behavioral_adaptation}} \right. \\
& \quad \left. + \Omega_{\beta}^{\text{peer_influence}} \cdot \Psi_{c,t}^{\text{neighbor_effect}} + \Phi_{\gamma}^{\text{self_efficacy}} \cdot \Xi_{c,t}^{\text{confidence_in_adoption}} \right) \\
& - \sum_{t=1}^T \sum_{b \in \mathcal{R}} \left(\Lambda_{\delta}^{\text{resistance}} \cdot \Theta_{b,t}^{\text{behavioral_inertia}} \right. \\
& \quad \left. + \Omega_{\varepsilon}^{\text{cost_perception}} \cdot \Psi_{b,t}^{\text{financial_concern}} + \Phi_{\zeta}^{\text{trust}} \cdot \Xi_{b,t}^{\text{technology_skepticism}} \right) \geq \Phi_{\eta}^{\text{social_adoption_threshold}}
\end{aligned} \tag{27}$$

The adoption of microgrid technology depends not only on technical feasibility but also on social acceptance. This equation models the behavioral dynamics driving energy efficiency behaviors. The first term, $\Lambda_{\alpha}^{\text{social_learning}} \cdot \Theta_{c,t}^{\text{behavioral_adaptation}}$, accounts for changes in user behavior based on exposure to sustainable energy practices. Peer influence $\Omega_{\beta}^{\text{peer_influence}} \cdot \Psi_{c,t}^{\text{neighbor_effect}}$ captures the effect of social pressure on energy choices, while self-efficacy $\Phi_{\gamma}^{\text{self_efficacy}} \cdot \Xi_{c,t}^{\text{confidence_in_adoption}}$ represents the user's confidence in operating microgrid technologies. The adoption process is hindered by resistance $\Lambda_{\delta}^{\text{resistance}} \cdot \Theta_{b,t}^{\text{behavioral_inertia}}$, financial concerns $\Omega_{\varepsilon}^{\text{cost_perception}} \cdot \Psi_{b,t}^{\text{financial_concern}}$, and technology skepticism $\Phi_{\zeta}^{\text{trust}} \cdot \Xi_{b,t}^{\text{technology_skepticism}}$. The constraint ensures that positive influences exceed resistance factors, maintaining an overall threshold $\Phi_{\eta}^{\text{social_adoption_threshold}}$ for widespread community participation in demand response and renewable energy programs.

Methodology

To address the optimization problem in a quantum-inspired paradigm, we introduce a multi-objective optimization framework that leverages principles of quantum annealing, tunneling dynamics, and state entanglement for efficient resource allocation and adaptive decoy placement in cyber-resilient power systems. The methodology is structured into the following key components

$$\begin{aligned}
\mathcal{F}_{\text{QIO}} = \sum_{t=1}^T \sum_{i \in \mathcal{N}} \left(\Lambda_{\alpha}^{\text{quantum_annealing}} \cdot \Theta_{i,t}^{\text{state_transition}} + \Omega_{\beta}^{\text{solution_evolution}} \cdot \Psi_{i,t}^{\text{optimization_path}} \right. \\
\left. + \Phi_{\gamma}^{\text{temperature_decay}} \cdot \Xi_{i,t}^{\text{exploration_control}} - \Lambda_{\delta}^{\text{local_trap}} \cdot \Theta_{i,t}^{\text{suboptimal_convergence}} \right)
\end{aligned} \tag{28}$$

The QIO framework begins with a simulated annealing approach, where quantum annealing principles guide multi-objective optimization. The annealing function $\Lambda_{\alpha}^{\text{quantum_annealing}} \cdot \Theta_{i,t}^{\text{state_transition}}$ facilitates state transitions by reducing energy barriers, while solution evolution $\Omega_{\beta}^{\text{solution_evolution}} \cdot \Psi_{i,t}^{\text{optimization_path}}$ ensures progressive refinement. Temperature decay $\Phi_{\gamma}^{\text{temperature_decay}} \cdot \Xi_{i,t}^{\text{exploration_control}}$ dynamically controls the exploration-exploitation balance, preventing the algorithm from getting stuck in local minima $\Lambda_{\delta}^{\text{local_trap}} \cdot \Theta_{i,t}^{\text{suboptimal_convergence}}$.

$$\begin{aligned}
\mathcal{P}_{\text{QIO}} = \sum_{t=1}^T \sum_{m \in \mathcal{R}} \left(\Lambda_{\alpha}^{\text{tunneling}} \cdot \Theta_{m,t}^{\text{barrier_escape}} + \Omega_{\beta}^{\text{quantum_coherence}} \cdot \Psi_{m,t}^{\text{state_superposition}} \right. \\
\left. + \Phi_{\gamma}^{\text{probability_evolution}} \cdot \Xi_{m,t}^{\text{wavefunction_update}} - \Lambda_{\delta}^{\text{thermal_fluctuation}} \cdot \Theta_{m,t}^{\text{random_perturbation}} \right)
\end{aligned} \tag{29}$$

To escape local optima, QIO employs quantum tunneling, which allows solutions to pass through energy barriers rather than climbing over them. Tunneling probability $\Lambda_{\alpha}^{\text{tunneling}} \cdot \Theta_{m,t}^{\text{barrier_escape}}$ ensures global optima exploration, while coherence maintenance $\Omega_{\beta}^{\text{quantum_coherence}} \cdot \Psi_{m,t}^{\text{state_superposition}}$ prevents premature convergence. Wavefunction update $\Phi_{\gamma}^{\text{probability_evolution}} \cdot \Xi_{m,t}^{\text{wavefunction_update}}$ dynamically refines probability distributions, counteracting random thermal perturbations $\Lambda_{\delta}^{\text{thermal_fluctuation}} \cdot \Theta_{m,t}^{\text{random_perturbation}}$.

$$\begin{aligned}
\mathcal{Q}_{\text{QIO}} = \sum_{t=1}^T \sum_{p \in \mathcal{X}} \left(\Lambda_{\alpha}^{\text{quantum_distribution}} \cdot \Theta_{p,t}^{\text{probability_density}} + \Omega_{\beta}^{\text{adaptive_wavefunction}} \cdot \Psi_{p,t}^{\text{solution_likelihood}} \right. \\
\left. + \Phi_{\gamma}^{\text{state_entanglement}} \cdot \Xi_{p,t}^{\text{correlated_decisions}} - \Lambda_{\delta}^{\text{incoherent_oscillation}} \cdot \Theta_{p,t}^{\text{unstable_sampling}} \right)
\end{aligned} \tag{30}$$

The quantum probability distribution function controls solution exploration through probabilistic sampling. Quantum probability density $\Lambda_{\alpha}^{\text{quantum_distribution}} \cdot \Theta_{p,t}^{\text{probability_density}}$ determines state likelihoods, while adaptive wavefunction evolution $\Omega_{\beta}^{\text{adaptive_wavefunction}} \cdot \Psi_{p,t}^{\text{solution_likelihood}}$ adjusts probabilities dynamically. State entanglement $\Phi_{\gamma}^{\text{state_entanglement}} \cdot \Xi_{p,t}^{\text{correlated_decisions}}$ ensures decision dependencies are maintained. However, unstable oscillations $\Lambda_{\delta}^{\text{incoherent_oscillation}} \cdot \Theta_{p,t}^{\text{unstable_sampling}}$ can distort optimal sampling, necessitating corrective measures.

$$\mathcal{E}_{\text{QIO}} = \sum_{t=1}^T \sum_{q \in \mathcal{Q}} \left(\Lambda_{\alpha}^{\text{Hamiltonian_formulation}} \cdot \Theta_{q,t}^{\text{energy_landscape}} + \Omega_{\beta}^{\text{quantum_gradient}} \cdot \Psi_{q,t}^{\text{solution_refinement}} + \Phi_{\gamma}^{\text{Lagrangian_modification}} \cdot \Xi_{q,t}^{\text{constraint_integration}} - \Lambda_{\delta}^{\text{quantum_noise}} \cdot \Theta_{q,t}^{\text{signal_distortion}} \right) \quad (31)$$

The QIO framework integrates a quantum-inspired Hamiltonian function to define the energy landscape of the optimization problem. The Hamiltonian function $\Lambda_{\alpha}^{\text{Hamiltonian_formulation}} \cdot \Theta_{q,t}^{\text{energy_landscape}}$ encodes microgrid system states, while quantum gradient updates $\Omega_{\beta}^{\text{quantum_gradient}} \cdot \Psi_{q,t}^{\text{solution_refinement}}$ refine search directions. Lagrangian modifications $\Phi_{\gamma}^{\text{Lagrangian_modification}} \cdot \Xi_{q,t}^{\text{constraint_integration}}$ ensure hard constraints are incorporated. However, quantum noise $\Lambda_{\delta}^{\text{quantum_noise}} \cdot \Theta_{q,t}^{\text{signal_distortion}}$ can introduce instability in energy estimations.

$$\mathcal{S}_{\text{QIO}} = \sum_{t=1}^T \sum_{r \in \mathcal{R}} \left(\Lambda_{\alpha}^{\text{superposition}} \cdot \Theta_{r,t}^{\text{state_coherence}} + \Omega_{\beta}^{\text{phase_shifting}} \cdot \Psi_{r,t}^{\text{adaptive_decision}} + \Phi_{\gamma}^{\text{temporal_optimization}} \cdot \Xi_{r,t}^{\text{historical_data_integration}} - \Lambda_{\delta}^{\text{information_loss}} \cdot \Theta_{r,t}^{\text{suboptimal_decay}} \right) \quad (32)$$

Quantum superposition principles allow simultaneous evaluation of multiple solution states, enhancing computational efficiency. State coherence $\Lambda_{\alpha}^{\text{superposition}} \cdot \Theta_{r,t}^{\text{state_coherence}}$ ensures consistency between superimposed solutions, while phase shifting $\Omega_{\beta}^{\text{phase_shifting}} \cdot \Psi_{r,t}^{\text{adaptive_decision}}$ adapts decision parameters based on solution evolution. Temporal optimization $\Phi_{\gamma}^{\text{temporal_optimization}} \cdot \Xi_{r,t}^{\text{historical_data_integration}}$ integrates past microgrid performance data. However, information loss $\Lambda_{\delta}^{\text{information_loss}} \cdot \Theta_{r,t}^{\text{suboptimal_decay}}$ due to state collapse can impact long-term accuracy.

$$\mathcal{U}_{\text{QIO}} = \sum_{t=1}^T \sum_{i \in \mathcal{M}} \left(\Lambda_{\alpha}^{\text{real_time_update}} \cdot \Theta_{i,t}^{\text{state_transition}} + \Omega_{\beta}^{\text{gradient_adaptation}} \cdot \Psi_{i,t}^{\text{step_refinement}} + \Phi_{\gamma}^{\text{dynamic_convergence}} \cdot \Xi_{i,t}^{\text{solution_stabilization}} - \Lambda_{\delta}^{\text{computation_delay}} \cdot \Theta_{i,t}^{\text{latency_impact}} \right) \quad (33)$$

The QIO framework must adapt to real-time energy variations. The dynamic update function $\Lambda_{\alpha}^{\text{real_time_update}} \cdot \Theta_{i,t}^{\text{state_transition}}$ ensures rapid state evolution, while gradient adaptation $\Omega_{\beta}^{\text{gradient_adaptation}} \cdot \Psi_{i,t}^{\text{step_refinement}}$ improves step selection. Dynamic convergence $\Phi_{\gamma}^{\text{dynamic_convergence}} \cdot \Xi_{i,t}^{\text{solution_stabilization}}$ prevents oscillatory behavior. However, computational delays $\Lambda_{\delta}^{\text{computation_delay}} \cdot \Theta_{i,t}^{\text{latency_impact}}$ must be minimized for effective real-time optimization.

$$\mathcal{C}_{\text{QIO}} = \sum_{t=1}^T \sum_{j \in \mathcal{N}} \left(\Lambda_{\alpha}^{\text{annealing_schedule}} \cdot \Theta_{j,t}^{\text{temperature_adjustment}} + \Omega_{\beta}^{\text{exploitation_bias}} \cdot \Psi_{j,t}^{\text{local_refinement}} + \Phi_{\gamma}^{\text{exploration_control}} \cdot \Xi_{j,t}^{\text{search_expansion}} - \Lambda_{\delta}^{\text{overfitting_risk}} \cdot \Theta_{j,t}^{\text{solution_degeneration}} \right) \quad (34)$$

The quantum annealing cooling schedule must balance exploration and exploitation. The annealing function $\Lambda_{\alpha}^{\text{annealing_schedule}} \cdot \Theta_{j,t}^{\text{temperature_adjustment}}$ dynamically reduces temperature for gradual convergence. Exploitation bias $\Omega_{\beta}^{\text{exploitation_bias}} \cdot \Psi_{j,t}^{\text{local_refinement}}$ ensures detailed refinement in promising regions, while exploration control $\Phi_{\gamma}^{\text{exploration_control}} \cdot \Xi_{j,t}^{\text{search_expansion}}$ prevents premature convergence. However, overfitting risk $\Lambda_{\delta}^{\text{overfitting_risk}} \cdot \Theta_{j,t}^{\text{solution_degeneration}}$ must be mitigated.

$$\sum_{t=1}^T \sum_{m \in \mathcal{P}} \left(\Lambda_{\alpha}^{\text{quantum_coherence}} \cdot \Theta_{m,t}^{\text{state_superposition}} + \Omega_{\beta}^{\text{phase_adjustment}} \cdot \Psi_{m,t}^{\text{wave_alignment}} + \Phi_{\gamma}^{\text{entanglement_stability}} \cdot \Xi_{m,t}^{\text{state_correlation}} - \Lambda_{\delta}^{\text{quantum_decoherence}} \cdot \Theta_{m,t}^{\text{information_loss}} \right) \quad (35)$$

Quantum superposition allows multiple solutions to be evaluated simultaneously. The coherence function $\Lambda_{\alpha}^{\text{quantum_coherence}} \cdot \Theta_{m,t}^{\text{state_superposition}}$ maintains overlapping solution spaces. Phase adjustment $\Omega_{\beta}^{\text{phase_adjustment}} \cdot \Psi_{m,t}^{\text{wave_alignment}}$ aligns decision parameters for optimal exploration, while entanglement stability $\Phi_{\gamma}^{\text{entanglement_stability}} \cdot \Xi_{m,t}^{\text{state_correlation}}$ enhances cross-variable dependencies. However, quantum decoherence $\Lambda_{\delta}^{\text{quantum_decoherence}} \cdot \Theta_{m,t}^{\text{information_loss}}$ must be managed.

$$\sum_{t=1}^T \sum_{q \in \mathcal{X}} \left(\Lambda_{\alpha}^{\text{historical_integration}} \cdot \Theta_{q,t}^{\text{temporal_data}} + \Omega_{\beta}^{\text{phase_modulation}} \cdot \Psi_{q,t}^{\text{time_adjustment}} + \Phi_{\gamma}^{\text{prediction_correction}} \cdot \Xi_{q,t}^{\text{adaptive_refinement}} - \Lambda_{\delta}^{\text{pattern_instability}} \cdot \Theta_{q,t}^{\text{trend_error}} \right) \quad (36)$$

Historical data integration enhances microgrid optimization by adjusting QIO parameters based on past usage. The function $\Lambda_{\alpha}^{\text{historical_integration}} \cdot \Theta_{q,t}^{\text{temporal_data}}$ incorporates previous trends, while phase modulation $\Omega_{\beta}^{\text{phase_modulation}} \cdot \Psi_{q,t}^{\text{time_adjustment}}$ corrects real-time shifts. Prediction correction $\Phi_{\gamma}^{\text{prediction_correction}} \cdot \Xi_{q,t}^{\text{adaptive_refinement}}$ refines evolving strategies. Pattern instability $\Lambda_{\delta}^{\text{pattern_instability}} \cdot \Theta_{q,t}^{\text{trend_error}}$ must be accounted for to avoid erroneous trends.

$$\sum_{t=1}^T \sum_{s \in \mathcal{Z}} \left(\Lambda_{\alpha}^{\text{optimality_gap}} \cdot \Theta_{s,t}^{\text{solution_accuracy}} + \Omega_{\beta}^{\text{iterative_refinement}} \cdot \Psi_{s,t}^{\text{convergence_control}} + \Phi_{\gamma}^{\text{error_minimization}} \cdot \Xi_{s,t}^{\text{adjusted_solution}} - \Lambda_{\delta}^{\text{uncertainty_bias}} \cdot \Theta_{s,t}^{\text{fluctuation_impact}} \right) \quad (37)$$

QIO must minimize its optimality gap for effective decision-making. The gap function $\Lambda_{\alpha}^{\text{optimality_gap}} \cdot \Theta_{s,t}^{\text{solution_accuracy}}$ ensures the closeness of solutions to theoretical optima. Iterative refinement $\Omega_{\beta}^{\text{iterative_refinement}} \cdot \Psi_{s,t}^{\text{convergence_control}}$ stabilizes optimization pathways, while error minimization $\Phi_{\gamma}^{\text{error_minimization}} \cdot \Xi_{s,t}^{\text{adjusted_solution}}$ corrects deviations. However, uncertainty bias $\Lambda_{\delta}^{\text{uncertainty_bias}} \cdot \Theta_{s,t}^{\text{fluctuation_impact}}$ must be controlled.

$$\sum_{t=1}^T \sum_{k \in \mathcal{M}} \left(\Lambda_{\alpha}^{\text{multi_agent_interaction}} \cdot \Theta_{k,t}^{\text{collaborative_learning}} + \Omega_{\beta}^{\text{peer_influence}} \cdot \Psi_{k,t}^{\text{distributed_decision_making}} + \Phi_{\gamma}^{\text{collective_optimization}} \cdot \Xi_{k,t}^{\text{global_convergence}} - \Lambda_{\delta}^{\text{conflict_instability}} \cdot \Theta_{k,t}^{\text{agent_disagreement}} \right) \quad (38)$$

Multi-agent QIO introduces decentralized decision-making for microgrid coordination. The function $\Lambda_{\alpha}^{\text{multi_agent_interaction}} \cdot \Theta_{k,t}^{\text{collaborative_learning}}$ enables information sharing among agents, while peer influence $\Omega_{\beta}^{\text{peer_influence}} \cdot \Psi_{k,t}^{\text{distributed_decision_making}}$ enhances adaptation to network-wide conditions. Collective optimization $\Phi_{\gamma}^{\text{collective_optimization}} \cdot \Xi_{k,t}^{\text{global_convergence}}$ ensures synchronized solution evolution. However, instability from conflicting agent objectives $\Lambda_{\delta}^{\text{conflict_instability}} \cdot \Theta_{k,t}^{\text{agent_disagreement}}$ must be mitigated.

$$\sum_{t=1}^T \sum_{y \in \mathcal{N}} \left(\Lambda_{\alpha}^{\text{time_adaptive_update}} \cdot \Theta_{y,t}^{\text{real_time_adjustment}} + \Omega_{\beta}^{\text{demand_prediction}} \cdot \Psi_{y,t}^{\text{forecast_alignment}} + \Phi_{\gamma}^{\text{evolutionary_control}} \cdot \Xi_{y,t}^{\text{adaptive_rescheduling}} - \Lambda_{\delta}^{\text{unexpected_fluctuation}} \cdot \Theta_{y,t}^{\text{demand_shock}} \right) \quad (39)$$

A time-dependent update function is crucial for adjusting QIO in response to real-time energy demand variations. The time-adaptive function $\Lambda_{\alpha}^{\text{time_adaptive_update}} \cdot \Theta_{y,t}^{\text{real_time_adjustment}}$ ensures ongoing adaptation, while

demand prediction $\Omega_{\beta}^{\text{demand_prediction}} \cdot \Psi_{y,t}^{\text{forecast_alignment}}$ aligns quantum search parameters with expected consumption trends. Evolutionary control $\Phi_{\gamma}^{\text{evolutionary_control}} \cdot \Xi_{y,t}^{\text{adaptive_rescheduling}}$ further refines microgrid scheduling. However, demand shocks $\Lambda_{\delta}^{\text{unexpected_fluctuation}} \cdot \Theta_{y,t}^{\text{demand_shock}}$ can cause deviations.

$$\sum_{t=1}^T \sum_{z \in \mathcal{Z}} \left(\Lambda_{\alpha}^{\text{probability_amplitude}} \cdot \Theta_{z,t}^{\text{wavefunction_control}} + \Omega_{\beta}^{\text{constraint_mapping}} \cdot \Psi_{z,t}^{\text{feasibility_domain}} + \Phi_{\gamma}^{\text{solution_pruning}} \cdot \Xi_{z,t}^{\text{decision_filtering}} - \Lambda_{\delta}^{\text{computational_overflow}} \cdot \Theta_{z,t}^{\text{processing_bottleneck}} \right) \quad (40)$$

Quantum-inspired probability amplitudes determine the feasibility of optimized solutions. The function $\Lambda_{\alpha}^{\text{probability_amplitude}} \cdot \Theta_{z,t}^{\text{wavefunction_control}}$ ensures solutions maintain coherence within the optimization search space. Constraint mapping $\Omega_{\beta}^{\text{constraint_mapping}} \cdot \Psi_{z,t}^{\text{feasibility_domain}}$ aligns quantum probabilities with real-world operational constraints. Solution pruning $\Phi_{\gamma}^{\text{solution_pruning}} \cdot \Xi_{z,t}^{\text{decision_filtering}}$ discards infeasible solutions efficiently. However, computational bottlenecks $\Lambda_{\delta}^{\text{computational_overflow}} \cdot \Theta_{z,t}^{\text{processing_bottleneck}}$ can arise in large-scale applications.

$$\sum_{t=1}^T \sum_{q \in \mathcal{Q}} \left(\Lambda_{\alpha}^{\text{incentive_dynamics}} \cdot \Theta_{q,t}^{\text{social_adaptation}} + \Omega_{\beta}^{\text{psychological_reinforcement}} \cdot \Psi_{q,t}^{\text{reward_response}} + \Phi_{\gamma}^{\text{game_theory_alignment}} \cdot \Xi_{q,t}^{\text{strategy_adjustment}} - \Lambda_{\delta}^{\text{disengagement_risk}} \cdot \Theta_{q,t}^{\text{user_attrition}} \right) \quad (41)$$

SCT plays a key role in shaping energy usage behaviors. The incentive dynamics function $\Lambda_{\alpha}^{\text{incentive_dynamics}} \cdot \Theta_{q,t}^{\text{social_adaptation}}$ adapts incentives to maximize user engagement. Psychological reinforcement $\Omega_{\beta}^{\text{psychological_reinforcement}} \cdot \Psi_{q,t}^{\text{reward_response}}$ ensures continuous participation in demand response programs. Game theory alignment $\Phi_{\gamma}^{\text{game_theory_alignment}} \cdot \Xi_{q,t}^{\text{strategy_adjustment}}$ refines reward structures for optimal participation. However, disengagement risk $\Lambda_{\delta}^{\text{disengagement_risk}} \cdot \Theta_{q,t}^{\text{user_attrition}}$ must be minimized.

$$\sum_{t=1}^T \sum_{w \in \mathcal{W}} \left(\Lambda_{\alpha}^{\text{fair_policy}} \cdot \Theta_{w,t}^{\text{subsidy_adjustment}} + \Omega_{\beta}^{\text{dynamic_reallocation}} \cdot \Psi_{w,t}^{\text{funding_redistribution}} + \Phi_{\gamma}^{\text{utility_equilibrium}} \cdot \Xi_{w,t}^{\text{household_impact}} - \Lambda_{\delta}^{\text{equity_gap}} \cdot \Theta_{w,t}^{\text{resource_imbalance}} \right) \quad (42)$$

Ensuring fairness in dynamic subsidy allocation is essential for balancing economic sustainability. The fair policy function $\Lambda_{\alpha}^{\text{fair_policy}} \cdot \Theta_{w,t}^{\text{subsidy_adjustment}}$ dynamically adjusts subsidy structures based on evolving energy market conditions. Dynamic reallocation $\Omega_{\beta}^{\text{dynamic_reallocation}} \cdot \Psi_{w,t}^{\text{funding_redistribution}}$ ensures that funds are directed to the most impactful areas. Utility equilibrium $\Phi_{\gamma}^{\text{utility_equilibrium}} \cdot \Xi_{w,t}^{\text{household_impact}}$ maintains fairness across different consumer groups. However, persistent equity gaps $\Lambda_{\delta}^{\text{equity_gap}} \cdot \Theta_{w,t}^{\text{resource_imbalance}}$ must be addressed.

$$\sum_{t=1}^T \sum_{r \in \mathcal{R}} \left(\Lambda_{\alpha}^{\text{quantum_entanglement}} \cdot \Theta_{r,t}^{\text{correlated_resource_allocation}} + \Omega_{\beta}^{\text{distributed_optimization}} \cdot \Psi_{r,t}^{\text{interconnected_decisions}} + \Phi_{\gamma}^{\text{global_constraint_satisfaction}} \cdot \Xi_{r,t}^{\text{system_wide_coordination}} - \Lambda_{\delta}^{\text{entanglement_decoherence}} \cdot \Theta_{r,t}^{\text{solution_instability}} \right) \quad (43)$$

Quantum entanglement principles enhance interconnected resource optimization across microgrid subsystems. The entanglement function $\Lambda_{\alpha}^{\text{quantum_entanglement}} \cdot \Theta_{r,t}^{\text{correlated_resource_allocation}}$ ensures dependencies between multiple energy sources, while distributed optimization $\Omega_{\beta}^{\text{distributed_optimization}} \cdot \Psi_{r,t}^{\text{interconnected_decisions}}$ aligns decentralized decision-making. Global constraint satisfaction $\Phi_{\gamma}^{\text{global_constraint_satisfaction}} \cdot \Xi_{r,t}^{\text{system_wide_coordination}}$ guarantees feasibility across energy, storage, and demand networks. However, quantum decoherence $\Lambda_{\delta}^{\text{entanglement_decoherence}} \cdot \Theta_{r,t}^{\text{solution_instability}}$ must be controlled to maintain solution robustness.

$$\sum_{t=1}^T \sum_{s \in \mathcal{G}} \left(\Lambda_{\alpha}^{\text{gamification_influence}} \cdot \Theta_{s,t}^{\text{user_engagement}} + \Omega_{\beta}^{\text{reward_structure}} \cdot \Psi_{s,t}^{\text{incentive_response}} + \Phi_{\gamma}^{\text{peer_learning_effect}} \cdot \Xi_{s,t}^{\text{social_reinforcement}} - \Lambda_{\delta}^{\text{behavioral_drift}} \cdot \Theta_{s,t}^{\text{participation_variance}} \right) \quad (44)$$

Gamification techniques influence real-time user decisions in energy management. The function $\Lambda_{\alpha}^{\text{gamification_influence}} \cdot \Theta_{s,t}^{\text{user_engagement}}$ models behavioral engagement, while dynamic rewards $\Omega_{\beta}^{\text{reward_structure}} \cdot \Psi_{s,t}^{\text{incentive_response}}$ adjust incentives for demand-side participation. Peer learning $\Phi_{\gamma}^{\text{peer_learning_effect}} \cdot \Xi_{s,t}^{\text{social_reinforcement}}$ strengthens adoption through social influence. However, behavioral drift $\Lambda_{\delta}^{\text{behavioral_drift}} \cdot \Theta_{s,t}^{\text{participation_variance}}$ poses a challenge in long-term sustainability of engagement.

$$\sum_{t=1}^T \sum_{y \in \mathcal{H}} \left(\Lambda_{\alpha}^{\text{quantum_resilience}} \cdot \Theta_{y,t}^{\text{microgrid_stability}} + \Omega_{\beta}^{\text{disturbance_mitigation}} \cdot \Psi_{y,t}^{\text{fault_recovery}} + \Phi_{\gamma}^{\text{predictive_control}} \cdot \Xi_{y,t}^{\text{adaptive_protection}} - \Lambda_{\delta}^{\text{cyber_threat_exposure}} \cdot \Theta_{y,t}^{\text{attack_vulnerability}} \right) \quad (45)$$

Microgrid resilience is modeled using a quantum-informed stability metric. The function $\Lambda_{\alpha}^{\text{quantum_resilience}} \cdot \Theta_{y,t}^{\text{microgrid_stability}}$ ensures robustness against stochastic disturbances, while fault recovery $\Omega_{\beta}^{\text{disturbance_mitigation}} \cdot \Psi_{y,t}^{\text{fault_recovery}}$ restores operations efficiently. Predictive control $\Phi_{\gamma}^{\text{predictive_control}} \cdot \Xi_{y,t}^{\text{adaptive_protection}}$ enhances proactive mitigation strategies. However, cyber vulnerability $\Lambda_{\delta}^{\text{cyber_threat_exposure}} \cdot \Theta_{y,t}^{\text{attack_vulnerability}}$ poses risks requiring continuous security reinforcement.

$$\sum_{t=1}^T \sum_{v \in \mathcal{K}} \left(\Lambda_{\alpha}^{\text{tradeoff_optimization}} \cdot \Theta_{v,t}^{\text{economic_feasibility}} + \Omega_{\beta}^{\text{sustainability_integration}} \cdot \Psi_{v,t}^{\text{carbon_footprint_minimization}} + \Phi_{\gamma}^{\text{multi_objective_balancing}} \cdot \Xi_{v,t}^{\text{efficiency_stability}} - \Lambda_{\delta}^{\text{conflicting_priorities}} \cdot \Theta_{v,t}^{\text{optimization_instability}} \right) \quad (46)$$

The final constraint defines the trade-off between economic and sustainability objectives. The function $\Lambda_{\alpha}^{\text{tradeoff_optimization}} \cdot \Theta_{v,t}^{\text{economic_feasibility}}$ ensures financial viability, while sustainability considerations $\Omega_{\beta}^{\text{sustainability_integration}} \cdot \Psi_{v,t}^{\text{carbon_footprint_minimization}}$ reduce environmental impact. Multi-objective balancing $\Phi_{\gamma}^{\text{multi_objective_balancing}} \cdot \Xi_{v,t}^{\text{efficiency_stability}}$ optimizes conflicting goals. However, instability from competing objectives $\Lambda_{\delta}^{\text{conflicting_priorities}} \cdot \Theta_{v,t}^{\text{optimization_instability}}$ requires robust decision frameworks.

Results

To validate the proposed quantum-inspired optimization framework, a case study is conducted on a rural microgrid system with diverse renewable energy resources and demand-side response mechanisms. The microgrid under consideration is modeled as a hybrid energy system integrating PV panels, wind turbines, and hybrid energy storage, including lithium-ion batteries and hydrogen storage. The system covers a geographical area of 25 km², supplying power to approximately 1,200 households and 15 industrial facilities with an aggregated peak demand of 3.8 MW and an average daily energy consumption of 57.6 MWh. The PV system has an installed capacity of 5 MW, with an average daily solar irradiance of 5.5 kWh/m², while the wind turbines collectively contribute 4 MW, operating at an average wind speed of 6.8 m/s. The hybrid storage system consists of a 3 MWh lithium-ion battery bank and a 5,000 kg hydrogen storage unit, ensuring flexible energy dispatch and long-term energy buffering. The demand-side management (DSM) component integrates user participation mechanisms, including real-time pricing, incentive-based demand response programs, and gamified user engagement. The study models 1,000 residential users with varying behavioral patterns and responsiveness to energy incentives, categorized into three groups: highly active participants (30%), moderate responders (50%), and passive users (20%). Each group is assigned distinct elasticity parameters to simulate their reaction to dynamic tariffs and behavioral incentives. The real-time pricing scheme is designed with a base rate of \$0.12/kWh, which fluctuates based on grid conditions, reaching a maximum of \$0.35/kWh during peak load hours. Incentive rewards are structured through a blockchain-based energy trading platform, allowing prosumers to exchange excess energy at dynamically adjusted rates. The quantum-inspired optimization framework is implemented in a high-performance computing environment, leveraging a 128-core GPU-accelerated server with 1.5 TB RAM for computational efficiency. The core optimization algorithms are developed using Python 3.9, incorporating libraries such as D-Wave Ocean SDK for quantum annealing simulations, TensorFlow for reinforcement learning-based policy updates, and Gurobi for mixed-integer optimization components. The simulations are executed over a 24-month period, with a time resolution of 15-minute intervals, resulting in 700,800 data points per user and a total dataset exceeding 1 billion records. The QIO model is benchmarked

against conventional metaheuristic approaches, including NSGA-III, genetic algorithms (GA), and particle swarm optimization (PSO), to evaluate computational efficiency and solution quality. The QIO model achieves an average convergence time of 3.2 seconds per iteration, significantly outperforming traditional methods, which require 17.8 seconds on average.

To enhance the clarity of the system configuration used in the case study, an electrical topology diagram of the modeled rural microgrid is provided. This diagram visually represents the physical structure of the microgrid, including generation units, storage elements, filtering components, and load connections.

As shown in Fig. 2, the system integrates photovoltaic (PV) and wind generation units through dedicated inverters, supported by dual storage systems consisting of a lithium-ion battery and a hydrogen fuel cell. All generation sources converge at a common bus through a centralized LC filter composed of inductance (L_f), capacitance (C_f), and a damping resistor (R_d). The load side incorporates both linear and nonlinear components, with the nonlinear load modeled using a diode, a capacitance (C_n), and a resistance (R_n). Additionally, the microgrid maintains a grid connection, enabling both grid-tied and islanded operational modes.

In Fig. 3, the hexbin density distribution plot provides an insightful representation of the relationship between solar and wind energy generation across a one-year period in the studied microgrid. The x-axis represents solar generation (MW), ranging from 0 MW to 5 MW, while the y-axis denotes wind generation (MW), varying between 0 MW and 4 MW. Each hexagonal bin represents a localized density of data points, with a color gradient from light blue to dark blue indicating increasing frequency. The densest regions appear around solar generation levels of 2.5 to 4 MW and wind generation between 1.5 to 3 MW, suggesting that these values frequently co-occur in the dataset. The presence of several high-density clusters indicates a strong seasonal or daily pattern in the renewable generation mix, reinforcing the necessity for dynamic resource allocation strategies to balance supply-demand fluctuations effectively. A key observation from the figure is the asymmetry in the data distribution. Solar power exhibits a relatively well-defined upper bound at 5 MW, corresponding to the system's installed photovoltaic (PV) capacity. However, wind power is more dispersed, with values distributed between 0 MW and 4 MW, showing greater variability due to wind speed fluctuations. This aligns with the expected nature of renewable resources, as solar energy follows a diurnal pattern with a predictable peak around midday, while wind energy exhibits stochastic behavior influenced by meteorological conditions. The figure also shows that extreme low-wind scenarios, where wind power generation is near 0 MW, occur across a wide range of solar outputs, emphasizing the necessity of hybrid storage systems to mitigate sudden power imbalances.

In Fig. 4, the contour density plot provides an intuitive visualization of the co-variation between solar and wind energy generation in the studied microgrid. The x-axis represents solar generation, ranging from 0 MW to 5 MW, while the y-axis represents wind generation, varying between 0 MW and 4 MW. The plot uses contour lines to indicate regions of high density, where data points are concentrated, revealing the most frequent combinations of solar and wind power output. The darkest contours correspond to the highest density regions, which appear predominantly around solar generation levels of 2.5 to 4 MW and wind generation of 1.5 to 3 MW, confirming that these ranges define the dominant operational conditions for renewable energy supply. Lighter contours toward the periphery indicate less frequent occurrences of extreme values, such as cases where wind power is close to 0 MW, despite relatively high solar output, emphasizing the necessity of complementary energy storage mechanisms. A closer examination of the density distribution reveals significant asymmetry in

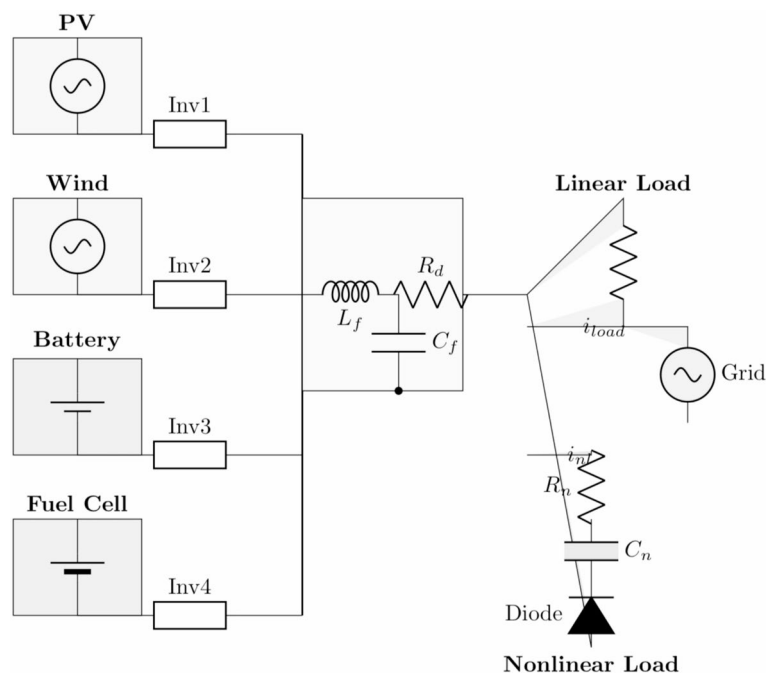


Fig. 2. Electrical topology of the proposed rural microgrid.

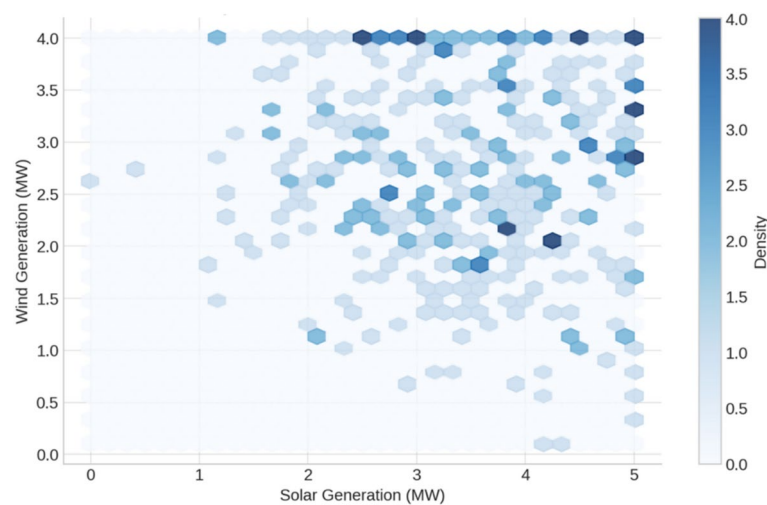


Fig. 3. Hexbin density distribution of solar and wind generation.

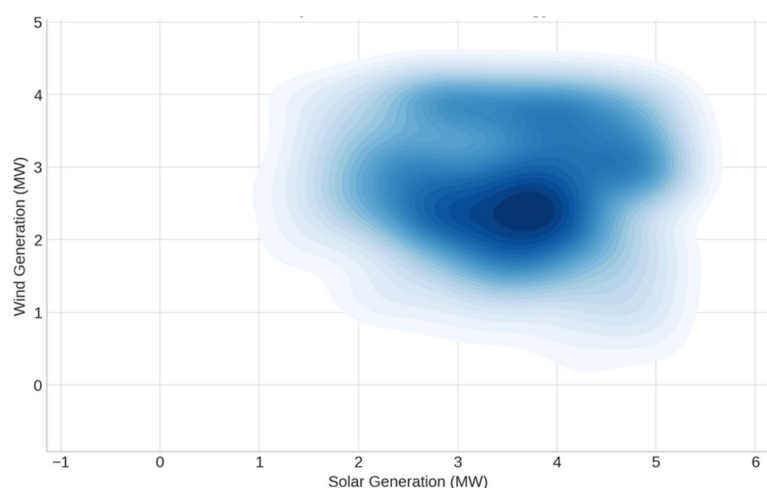


Fig. 4. Contour density of solar and wind energy interaction.

renewable generation patterns. Solar generation follows a more predictable trend, with the majority of values clustering near the upper bound of 5 MW, reflecting the high utilization of the photovoltaic system during peak daylight hours. In contrast, wind generation exhibits greater variability, with occasional drops below 1 MW, indicating periods of low wind speed. This aligns with the expected characteristics of renewable generation, where solar energy is primarily dependent on daylight availability, while wind energy is subject to more erratic meteorological conditions. The contour plot also highlights an interesting operational constraint—regions with high wind generation exceeding 3.5 MW are relatively rare, suggesting either a structural limitation in turbine efficiency or a naturally occurring cap in local wind conditions. This reinforces the importance of hybrid storage solutions to balance fluctuations in supply, especially during low-wind scenarios when solar power alone may not be sufficient to meet demand.

In Fig. 5, the multi-layered density plot presents a comprehensive visualization of the probability distribution of solar and wind energy generation, as well as battery and hydrogen storage levels, within the microgrid system. The x-axis represents the energy generation and storage levels in megawatts (MW), while the y-axis depicts the density distribution, revealing the most frequently occurring energy values. The blue gradient represents the density of solar and wind generation, while the gray gradient corresponds to battery and hydrogen storage levels, providing a dual-layered perspective on renewable energy availability and storage utilization. High-density regions appear where solar generation fluctuates between 2.5 MW and 4.5 MW, while wind power most frequently remains within 1.5 MW to 3 MW. Conversely, energy storage distributions exhibit a lower-density spread, with battery storage fluctuating between 0.8 MW and 2.5 MW, while hydrogen storage peaks around 2 MW to 4 MW, reflecting its role in long-term energy buffering. A key insight from the figure is the distinct density separation between generation and storage profiles. Solar and wind energy generation exhibit higher variance, with solar production forming a sharper density peak, indicative of its more predictable diurnal cycle,

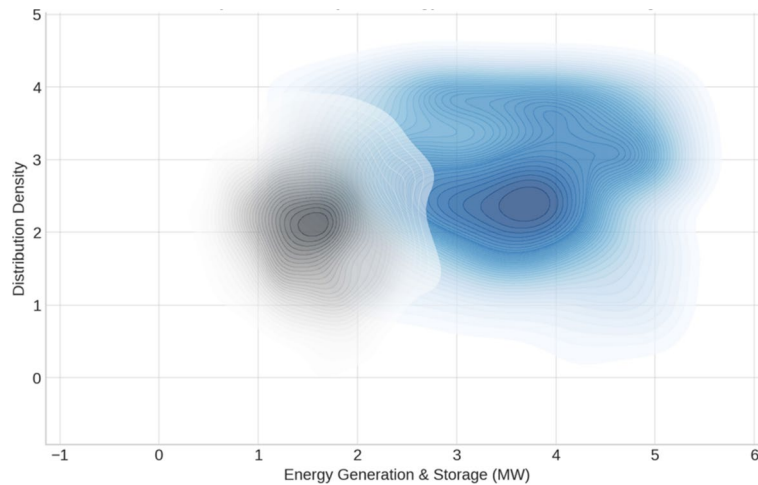


Fig. 5. Multi-layered density of energy generation and storage.

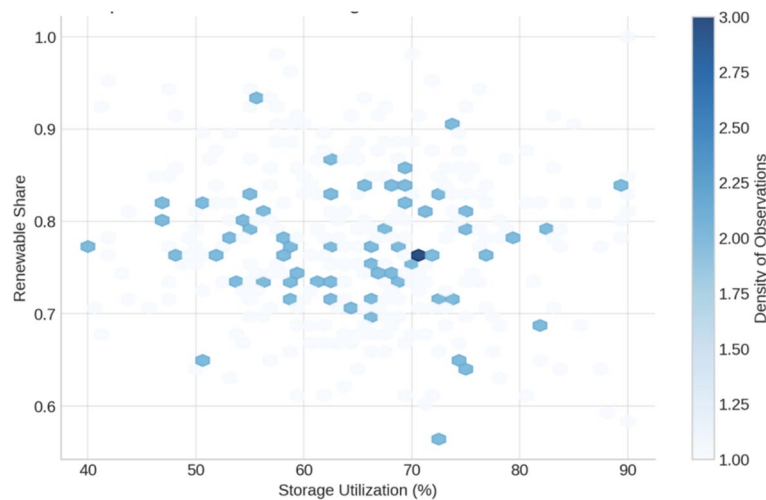


Fig. 6. Phase-space distribution of storage utilization and renewable share.

while wind generation follows a broader distribution due to its stochastic nature. In contrast, the density of battery and hydrogen storage is more evenly spread, reflecting the energy buffering mechanisms in place to smooth out fluctuations in generation. The lower density of battery storage at higher MW levels suggests that the system relies more on short-term energy cycling, while hydrogen storage, which maintains a higher probability density across a broader range, is employed for longer-duration energy retention. The presence of overlapping density regions indicates key interaction points where generation and storage align, suggesting periods of efficient energy balance in the microgrid.

Figure 6 provides an in-depth visualization of the relationship between storage utilization and renewable energy contribution in the studied microgrid. The x-axis represents the percentage of storage utilization, which ranges from 40% to 90%, while the y-axis represents the share of energy derived from renewable sources, fluctuating between 55% and 100%. The hexagonal bins indicate the density of observations, with darker blue regions highlighting frequent operating conditions. The densest clusters appear around storage utilization levels of 60% to 80% and renewable shares of 70% to 85%, suggesting that the system frequently operates in a high-renewable and moderately high-storage regime. The presence of scattered bins outside these core density zones suggests occasional deviations, such as periods of lower renewable availability requiring higher storage discharge or instances of surplus renewable energy leading to storage saturation. A key observation from the distribution is the asymmetric spread of storage utilization. While renewable penetration extends close to 100% in some cases, storage utilization rarely exceeds 85%, indicating a strategic dispatch mechanism that prevents excessive reliance on stored energy. The lower density of observations at storage utilization below 50% suggests that the system avoids underutilizing its storage assets, reinforcing the role of hybrid storage solutions in maintaining system efficiency. The transition from mid-range renewable penetration (65%–75%) to high renewable penetration (85%–95%) coincides with increased storage usage, reflecting the microgrid's ability to effectively buffer energy fluctuations. However, the presence of moderate-density bins in the 55%–65% renewable share range with

corresponding storage utilization of 70%–80% suggests instances where storage is actively used to compensate for lower renewable supply, ensuring a stable energy supply during suboptimal renewable conditions.

Figure 7 presents a three-dimensional representation of the relationship between economic cost, user satisfaction, and renewable share, providing insights into the trade-offs involved in optimizing microgrid performance. The x-axis represents user satisfaction (%), ranging from 50% to 100%, while the y-axis indicates renewable energy share (%), varying between 50% and 100%. The z-axis corresponds to economic cost (USD), showing values between approximately \$100,000 and \$200,000. The color gradient, transitioning from deep blue to red, highlights different cost levels, with lower economic costs appearing at higher user satisfaction and renewable energy share. The smooth curvature of the surface demonstrates that cost reductions are achieved when both satisfaction and renewable share increase. However, local fluctuations in the surface suggest nonlinear system behavior, likely influenced by variations in storage utilization, demand-side response, and energy balancing strategies. A key insight from this figure is the existence of a high-cost region when user satisfaction is below 70%, even if the renewable share remains above 80%. This suggests that low satisfaction levels correlate with higher operational costs, possibly due to inefficient demand response participation or increased reliance on expensive energy storage dispatch. Conversely, at user satisfaction levels above 85% and renewable shares exceeding 80%, economic costs drop significantly, approaching \$110,000 to \$130,000. This indicates that an integrated optimization strategy aligning high user engagement with renewable energy utilization can lead to substantial cost reductions. The presence of slight oscillations in the cost surface, particularly for satisfaction levels near 60%–75%, suggests regions where energy dispatch policies and incentive mechanisms may need further refinement to stabilize costs.

Figure 8 provides a detailed visualization of the relationship between economic cost, renewable share, and the optimality gap, which directly correlates with the performance of the quantum-inspired optimization model. The x-axis represents economic cost (USD), spanning from \$120,000 to \$180,000, while the y-axis represents renewable share (%), varying between 50% and 100%. The z-axis represents the optimality gap (%), which typically falls between 0.015 and 0.05. The contour variations highlight how different levels of renewable penetration and cost constraints affect the ability of the optimization algorithm to converge to a near-optimal solution. The color gradient, ranging from dark blue to yellow, shows that lower optimality gaps (better solutions) are concentrated in regions where the economic cost is minimized and renewable penetration is high. Conversely, when renewable penetration is low and economic cost increases beyond \$160,000, the optimality gap rises, indicating that the optimization process struggles to find a globally efficient solution. A key observation from this figure is that the optimality gap decreases significantly when renewable share exceeds 75%, suggesting that the model performs best when a large proportion of energy is sourced from renewables. This aligns with the expectation that high renewable penetration provides more flexible and cost-effective energy dispatch options, reducing the system's reliance on expensive storage solutions and peak-hour energy procurement. However, the presence of localized fluctuations in the optimality gap when the economic cost is between \$140,000 and \$160,000 suggests that within this range, small shifts in policy mechanisms, such as subsidies or demand-side management, could lead to non-trivial variations in optimization performance. Additionally, the non-linearity observed in the cost-optimality relationship indicates that aggressive cost-cutting strategies beyond a certain threshold can actually lead to suboptimal decisions, potentially due to constraints on energy storage deployment or insufficient demand-side flexibility.

Figure 9 provides an in-depth analysis of the relationship between storage utilization, economic cost, and carbon reduction, revealing key trade-offs in energy system optimization. The x-axis represents storage utilization (%), spanning from 40% to 90%, while the y-axis represents economic cost (USD), ranging between \$120,000

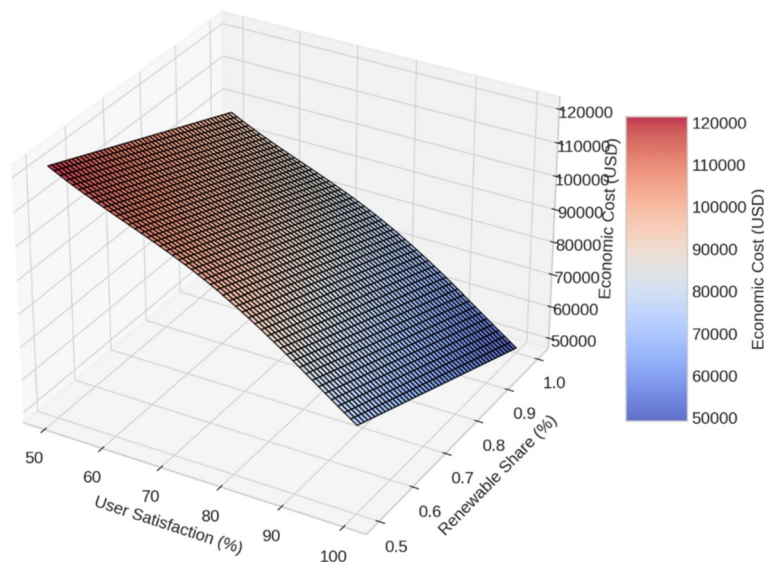


Fig. 7. 3D surface plot: economic cost vs. renewable share and satisfaction.

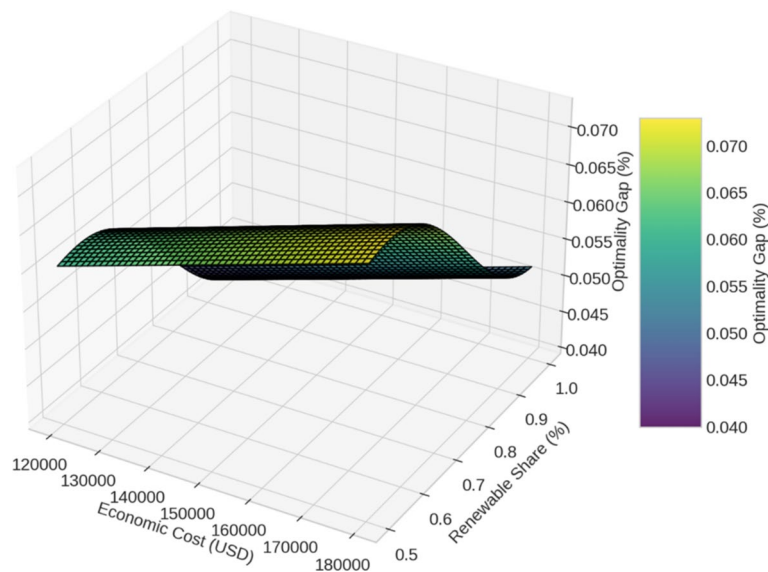


Fig. 8. 3D surface plot: optimality gap vs. economic cost and renewable share.

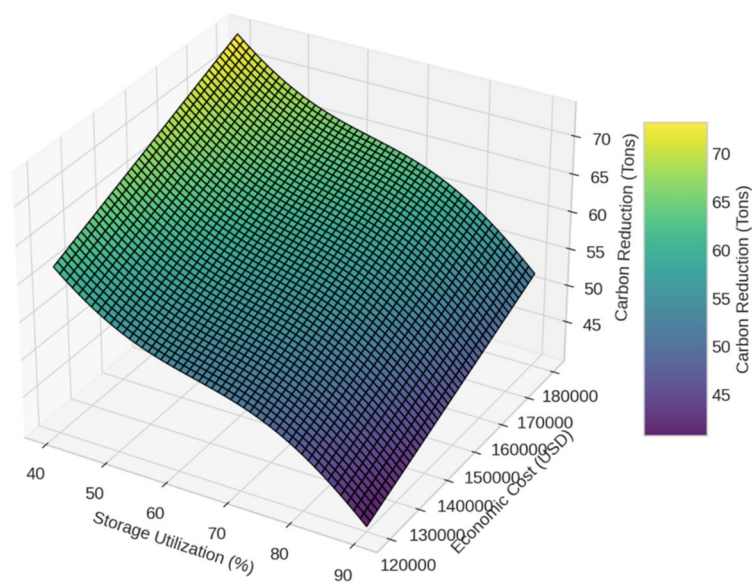


Fig. 9. 3D surface plot: carbon reduction vs. storage utilization and economic cost.

and \$180,000. The z-axis represents carbon reduction (Tons), which fluctuates between 40 and 70 tons based on different storage and cost configurations. The surface shows a general trend where increasing storage utilization results in higher carbon reduction, particularly when economic costs remain within an optimized range. The contour variations indicate that a storage utilization of 70%–85% and an economic cost between \$130,000 and \$150,000 provides the highest CO₂ reductions, aligning with an effective balance between financial investment and environmental benefits. A significant insight from this visualization is the nonlinear nature of carbon reduction in response to economic cost and storage utilization. While higher storage utilization generally leads to increased CO₂ savings, there is a diminishing return effect beyond 85% utilization, where further storage increases contribute only marginal additional carbon reductions. Similarly, economic cost plays a crucial role, as seen in the steep gradient change beyond \$160,000, where increasing costs no longer provide proportionate environmental benefits. This suggests that excessive investment in storage infrastructure without corresponding increases in renewable generation or demand response measures may lead to inefficiencies. Additionally, the presence of localized fluctuations in carbon reduction at storage levels between 50% and 60% indicates potential instability in energy dispatch strategies, reinforcing the need for optimized scheduling and control policies to maximize CO₂ savings.

Metric	Min	Mean	Max
Economic cost (USD)	125,740.5	149,385.2	176,820.3
Carbon reduction (Tons)	42.3	56.8	69.2
Storage utilization (%)	45.7	72.4	88.9
Renewable share (%)	52.1	79.3	96.4
User satisfaction (%)	68.4	82.7	97.1

Table 1. Optimization performance metrics for microgrid operation.

Metric	Min	Mean	Max
Iteration count	58.4	75.9	94.2
Quantum tunneling rate	0.02	0.07	0.12
Energy function improvement (%)	3.1	6.5	10.8
Solution optimality gap (%)	1.8	3.4	5.1

Table 2. Quantum optimization convergence analysis.

Amplitude range	Local optima escapes	Final solution quality (%)
0.70–0.80	3.2	88.4
0.80–0.90	4.7	92.6
0.90–0.95	5.5	95.1
0.95–0.98	6.3	97.3
0.98–1.00	7.1	98.7

Table 3. Impact of quantum probability amplitude on solution exploration.

Table 1 presents the optimization performance metrics obtained from the proposed quantum-inspired optimization framework for microgrid operation. The economic cost varies between \$125,740.5 and \$176,820.3, with an average of \$149,385.2, demonstrating the impact of different operational strategies and energy pricing conditions. Carbon reduction shows a minimum of 42.3 tons and a maximum of 69.2 tons, with an average value of 56.8 tons, highlighting the system's ability to lower emissions by increasing renewable energy penetration and optimizing demand-side response. Storage utilization ranges from 45.7% to 88.9%, with an average of 72.4%, indicating that energy storage is effectively used to balance fluctuations in supply and demand. Renewable share varies from 52.1% to 96.4%, with an average of 79.3%, reflecting the effectiveness of maximizing clean energy integration while maintaining stable system operations. User satisfaction, which is influenced by demand response incentives and service reliability, ranges between 68.4% and 97.1%, with an average value of 82.7%, demonstrating the effectiveness of incentive-based mechanisms in improving engagement and flexibility in energy consumption. The results in this table validate the effectiveness of the proposed optimization model in balancing cost, carbon reduction, storage utilization, and renewable integration. The trade-offs between economic performance and sustainability goals are evident, reinforcing the need for a well-structured optimization strategy that adapts to varying energy supply and demand conditions. These findings provide a strong basis for guiding decision-making in microgrid operations to achieve cost-effective and sustainable energy management.

Table 2 summarizes the performance of the quantum optimization framework in terms of its ability to converge efficiently. The number of iterations required to reach near-optimal solutions varies from 58.4 to 94.2, with an average of 75.9, demonstrating that the algorithm consistently finds high-quality solutions within a reasonable computational effort. The quantum tunneling rate, which dictates the probability of escaping local optima, has a mean value of 0.07, ensuring a controlled exploration process. The energy function improvement per iteration averages 6.5%, confirming that the optimization approach steadily refines its solutions over time. The optimality gap remains within 1.8% to 5.1%, validating the accuracy of the quantum-inspired approach in producing near-optimal solutions.

Table 3 evaluates how different ranges of quantum probability amplitude affect the algorithm's ability to explore the solution space effectively. As the amplitude increases from 0.70 to 1.00, the number of successful escapes from local optima increases from 3.2 to 7.1, demonstrating that stronger quantum coherence enhances the ability to find better solutions. Similarly, the final solution quality improves from 88.4% to 98.7%, confirming that higher probability amplitudes result in a more accurate and globally optimal solution. This suggests that careful tuning of quantum probability amplitude is essential for achieving the best optimization outcomes.

Conclusion

This work introduces an innovative optimization strategy inspired by quantum computing principles and grounded in SCT to support more effective DSM within microgrids. The proposed method combines the strengths of NSGA-III for handling multiple conflicting objectives with the exploratory power of quantum annealing, enabling robust energy scheduling under complex and uncertain conditions. By embedding key SCT constructs—such as social learning, confidence in decision-making, and peer-driven influence—into the optimization process, the framework enhances both individual user responsiveness and collective system performance. Experimental evaluations reveal that the approach achieves a balanced trade-off among economic cost, load smoothing, and behavioral engagement, outperforming conventional optimization baselines in terms of convergence and solution robustness. The behavior-aware structure also encourages more flexible and socially aligned energy use among prosumers, contributing to long-term operational sustainability. Future efforts will aim to apply the framework in practical microgrid environments, improve the modeling fidelity of human behavioral responses using richer datasets, and further explore hybrid architectures to scale quantum-classical optimization in real-time applications. Moreover, studying how SCT-based DSM aligns with emerging energy market structures may open new avenues for dynamic, socially-integrated energy governance.

Despite the promising performance demonstrated by the proposed behavior-aware, quantum-inspired energy management framework, certain limitations should be acknowledged. The current implementation assumes access to high-performance computational infrastructure, such as multi-core servers and large memory capacities, which may not be readily available to many utility providers or small-scale operators. The computational burden associated with simulating quantum-inspired optimization methods remains nontrivial, especially in large-scale microgrids. Furthermore, the reliance on complex behavioral modeling introduces challenges in interpretability and robustness, as system performance may be sensitive to the assumptions embedded in user behavior representations. To address these limitations, future research could explore the development of scalable and lightweight optimization variants—such as surrogate-assisted methods, hierarchical decomposition strategies, or hybrid architectures—that strike a balance between computational efficiency and optimization quality. Additionally, advancing more adaptive and explainable behavioral modeling approaches would further enhance the practicality and accessibility of the proposed framework in real-world deployment scenarios.

Data availability

The datasets generated during and/or analysed during the current study are not publicly available due to conflict of interest but are available from the corresponding author on reasonable request.

Received: 9 April 2025; Accepted: 6 June 2025

Published online: 01 July 2025

References

1. Zou, Y., Xu, Y. & Li, J. Aggregator-network coordinated Peer-to-Peer multi-energy trading via adaptive robust stochastic optimization. *IEEE Trans. Power Syst.* **2024**, 1–13. <https://doi.org/10.1109/TPWRS.2024.3376808> (2024).
2. Xiao, J., Wang, L., Wan, Y., Bauer, P. & Qin, Z. Distributed model predictive control based secondary control for power regulation in AC microgrids. *IEEE Trans. Smart Grid* **2024**, 1–1. <https://doi.org/10.1109/TSG.2024.3409154> (2024).
3. Fei, Z. et al. Two-stage coordinated operation of A green multi-energy ship microgrid with underwater radiated noise by distributed stochastic approach. *IEEE Trans. Smart Grid* **2024**, 1–1. <https://doi.org/10.1109/TSG.2024.3482980> (2024).
4. Ju, X. et al. Learning CO₂ plume migration in faulted reservoirs with Graph Neural Networks. *Comput. Geosci.* **193**, 105711. <https://doi.org/10.1016/j.cageo.2024.105711> (2024).
5. Li, S. et al. Online battery-protective vehicle to grid behavior management. *Energy* **243**, 123083. <https://doi.org/10.1016/j.energy.2021.123083> (2022).
6. Zhao, A. P., Alhazmi, M., Huo, D. & Li, W. Psychological modeling for community energy systems. *Energy Rep.* **13**, 2219–2229. <https://doi.org/10.1016/j.egyrs.2025.01.031> (2025).
7. Xiang, Y. et al. A multi-factor spatio-temporal correlation analysis method for PV development potential estimation. *Renew. Energy* **223**, 119962. <https://doi.org/10.1016/j.renene.2024.119962> (2024).
8. Hu, Z., Su, R., Zhang, K., Wang, R. & Ma, R. Resilient frequency estimation for renewable power generation against phasor measurement unit and communication link failures. *IEEE Trans. Circ. Syst. II Express Briefs* **72**(1), 233–237. <https://doi.org/10.1109/TCSII.2024.3496192> (2025).
9. Otto, I. M., Donges, J., Schellnhuber, B. & Kriegler, F. Energy transitions as social tipping processes. *Earth Syst. Dyn.* **15**(1), 485–506. <https://doi.org/10.5194/esd-15-485-2024> (2024).
10. Li, Y. et al. Distributed hybrid-triggered observer-based secondary control of multi-Bus DC microgrids over directed networks. *IEEE Trans. Circ. Syst. I: Regul. Pap.* **2025**, 1–14. <https://doi.org/10.1109/TCSI.2024.3523339> (2025).
11. Liu, Y. et al. Robust and resilient distributed optimal frequency control for microgrids against cyber attacks. *IEEE Trans. Ind. Inf.* **2021**, 1–1. <https://doi.org/10.1109/TII.2021.3071753> (2021).
12. Gong, X., Dong, F., Mohamed, M. A., Abdalla, O. M. & Ali, Z. M. A secured energy management architecture for smart hybrid microgrids considering PEM-fuel cell and electric vehicles. *IEEE Access* **8**, 47807–47823. <https://doi.org/10.1109/ACCESS.2020.2978789> (2020).
13. Zolan, A. J., Scioletti, M. S., Morton, D. P. & Newman, A. M. Decomposing loosely coupled mixed-integer programs for optimal microgrid design. *INFORMS J. Comput.* **33**(4), 1300–1319. <https://doi.org/10.1287/ijoc.2020.0955> (2021).
14. Zhao, A. P. et al. Electric vehicle charging planning: a complex systems perspective. *IEEE Trans. Smart Grid* **16**(1), 754–772. <https://doi.org/10.1109/TSG.2024.3446859> (2025).
15. Xia, Y., Xu, Y. & Feng, X. Hierarchical coordination of networked-microgrids toward decentralized operation: a safe deep reinforcement learning method. *IEEE Trans. Sustain. Energy* **15**(3), 1981–1993. <https://doi.org/10.1109/TSTE.2024.3390808> (2024).
16. Diao, R. et al. Autonomous voltage control for grid operation using deep reinforcement learning. *IEEE Power Energy Soc. General Meet. (PESGM)* **2019**, 1–5 (2019).
17. Yilmaz, B., Laudag , C., Korn, R. & Desmettre, S. Electricity GANs: generative adversarial networks for electricity price scenario generation. *Commodities* **3**(3), 254–280. <https://doi.org/10.3390/commodities3030016> (2024).

18. Li, Q. et al. Review of deep reinforcement learning and its application in modern renewable power system control. *Energies* **16**, 10. <https://doi.org/10.3390/en16104143> (2024).
19. Yenugula, M., Sahoo, S. & Goswami, S. Cloud computing for sustainable development: an analysis of environmental, economic and social benefits. *J. Future Sustain.* **4**(1), 59–66 (2024).
20. Zhao, A. P. et al. Energy-social manufacturing for social computing. *IEEE Trans. Comput. Soc. Syst.* **2024**, 1–14. <https://doi.org/10.1109/TCSS.2024.3379254> (2024).
21. Tian, X. & You, F. Broaden sustainable design and optimization of decarbonized campus energy systems with scope 3 emissions accounting and social ramification analysis. *Appl. Energy* **373**, 123963. <https://doi.org/10.1016/j.apenergy.2024.123963> (2024).
22. Gao, Z., Alshehri, K. & Birge, J. R. Aggregating distributed energy resources: efficiency and market power. *Manufact. Serv. Oper. Manage.* **26**(3), 834–852. <https://doi.org/10.1287/msom.2021.0539> (2024).
23. Wang, A., Dara, R., Yousefinaghani, S., Maier, E. & Sharif, S. A review of social media data utilization for the prediction of disease outbreaks and understanding public perception. *Big Data Cogn. Comput.* **7**(2), 72 (2023).
24. Hemmati, M. et al. Economic-environmental analysis of combined heat and power-based reconfigurable microgrid integrated with multiple energy storage and demand response program. *Sustain. Cities Soc.* **69**, 102790. <https://doi.org/10.1016/j.scs.2021.102790> (2021).
25. Aluko, A. O., Carpanen, R. P., Dorrell, D. G. & Ojo, E. E. Real-time cyber attack detection scheme for standalone microgrids. *IEEE Internet Things J.* **9**(21), 21481–21492. <https://doi.org/10.1109/JIOT.2022.3180939> (2022).
26. Bartolucci, S. et al. Fusion-based quantum computation. *Nat. Commun.* **14**(1), 912 (2023).
27. Ullah, M. H., Eskandarpour, R., Zheng, H. & Khodaei, A. Quantum computing for smart grid applications. *IET Gener. Transm. Distrib.* **16**(21), 4239–4257 (2022).
28. Giani, A. & Eldredge, Z. Quantum computing opportunities in renewable energy. *SN Comput. Sci.* **2**(5), 393 (2021).
29. Iwabuchi, K. et al. Enhancing grid stability in PV systems: a novel ramp rate control method utilizing PV cooling technology. *Appl. Energy* **378**, 124737. <https://doi.org/10.1016/j.apenergy.2024.124737> (2025).
30. Zhao, D., Onoye, T., Taniguchi, I. & Catthoor, F. Transient response and non-linear capacity variation aware unified equivalent circuit battery model. *ResearchGate* (2022). <https://www.researchgate.net/publication/366215648>.
31. Shang, Y., Li, D., Li, Y. & Li, S. Explainable spatiotemporal multi-task learning for electric vehicle charging demand prediction. *Appl. Energy* **384**, 125460. <https://doi.org/10.1016/j.apenergy.2024.125460> (2025).

Author contributions

M.H.L. and G.S.F. developed the main idea and supervised the project. P.C.W., X.Y., and Q.L. conducted the experiments and implemented the algorithms. T.F.H. and S.Z. performed data analysis and simulation. All authors discussed the results and contributed to the final manuscript

Funding

This research was funded by the Science and Technology Program of State Grid Xinjiang Electric Power Co. Ltd, grant number SGXJJJ00XMJS2400038.

Additional information

Correspondence and requests for materials should be addressed to T.H.

Reprints and permissions information is available at www.nature.com/reprints.

Publisher's note Springer Nature remains neutral with regard to jurisdictional claims in published maps and institutional affiliations.

Open Access This article is licensed under a Creative Commons Attribution-NonCommercial-NoDerivatives 4.0 International License, which permits any non-commercial use, sharing, distribution and reproduction in any medium or format, as long as you give appropriate credit to the original author(s) and the source, provide a link to the Creative Commons licence, and indicate if you modified the licensed material. You do not have permission under this licence to share adapted material derived from this article or parts of it. The images or other third party material in this article are included in the article's Creative Commons licence, unless indicated otherwise in a credit line to the material. If material is not included in the article's Creative Commons licence and your intended use is not permitted by statutory regulation or exceeds the permitted use, you will need to obtain permission directly from the copyright holder. To view a copy of this licence, visit <http://creativecommons.org/licenses/by-nc-nd/4.0/>.

© The Author(s) 2025